
Weak value description of an Interferometer and its Application

Katharina Senkalla



Munich 2018

Weak value description of an Interferometer and its Application

Katharina Senkalla

MASTER THESIS
at Department of Physics
Ludwig–Maximilians–University
Munich

Chair of Prof. Dr. Theodor W. Hänsch
Working group of Prof. Dr. Harald Weinfurter

submitted by
Katharina Senkalla

Munich, 23.03.2018

Supervisor: Prof. Dr. Harald Weinfurter

Weak-Value-Beschreibung eines Interferometers und deren Anwendung

MASTERARBEIT
an der Fakultät für Physik
Ludwig-Maximilians-Universität
München

Lehrstuhl von Prof. Dr. Theodor W. Hänsch
Arbeitsgruppe von Prof. Dr. Harald Weinfurter

eingereicht von
Katharina Senkalla

München, 23.03.2018

Betreuer: Prof. Dr. Harald Weinfurter

Abstract

In 1988 Aharonov, Albert, and Vaidman introduced the weak value concept, which allows to characterize the weak interaction of pre- and postselected quantum systems with external systems, also called *pointers* according to the von Neumann measurement model. In this thesis it is shown theoretically and in an interferometer experiment that the concept provides a simple and yet universal description for the modification of effects observable after various interactions of the system with the corresponding pointer systems, namely that the shifts in the expectation values of the different pointer observables are all changed in the same manner described by the weak value. This universality property of the weak value is demonstrated by considering a photon in an interferometer with weak local interactions between the path degree of freedom, which is the system, and other degrees of freedom, such as position, momentum, and polarization of the photon, which are the pointer systems. Furthermore, interpreting the misalignment of an interferometer as interaction in position and momentum inspired an easily accessible and efficient alignment technique, which is based on the evaluation of the interference pattern. We exploit the fact that its phase dependent centroid position is modified according to the also phase dependent weak value.

Contents

1	Introduction	1
2	Fundamental principles	3
2.1	Quantum measurements	3
2.1.1	Projective measurements	3
2.1.2	Generalization of the projection postulate	4
2.1.3	Von Neumann measurement model	5
2.2	Two-state vector formalism	7
2.2.1	Measurements on pre- and postselected systems	7
2.2.2	The weak value	9
2.2.3	Weak value amplification	10
3	Experimental framework	13
3.1	The different experimental parts	14
3.1.1	Laser System	14
3.1.2	Laser Monitoring	14
3.1.3	Interferometer	14
3.1.4	Spatial Detection	15
3.1.5	Polarization Analysis	16
3.2	Geometrical considerations	17
3.2.1	Obtaining the spatial and angular displacement	17
3.2.2	Setting the spatial and angular displacement	18
4	Universality of weak values	21
4.1	Introduction	21
4.2	Theoretical considerations	21
4.2.1	Calculation of the weak value	23
4.2.2	External systems in interferometric PPS	25
4.2.3	New insights in the change of expectation values	26
4.3	Experimental demonstration	30
4.3.1	Introducing the various interactions	30
4.3.2	Observation of the universality of the weak value	32
4.3.3	Parameter dependence of modified weak value	35

4.4	Conclusion	37
5	Alignment of interferometers using weak values	39
5.1	Introduction	39
5.2	Theoretical considerations	40
5.2.1	Gaussian pointers considered for strong interactions	40
5.2.2	Misalignment as interaction	41
5.2.3	Derivation of the fit function	43
5.3	Experimental demonstration	43
5.3.1	Alignment procedure	43
5.3.2	Discussion	47
5.4	Conclusion	48
6	Summary and outlook	49
	Appendices	51
	Appendix A Setup	53
A.1	Optical components	53
A.1.1	Polarizers	53
A.1.2	Waveplates	53
A.1.3	Yttrium-vanadate crystals	54
A.1.4	Beam splitter	54
A.1.5	Fabry-Pérot cavity	55
A.2	Methods	55
A.2.1	Phase correction	55
A.2.2	Estimation of position error	57
	Appendix B Mathematical calculations	59
B.1	Derivation of mixed state of the system	59
B.2	Derivation of the state of postselected external systems (omitting normalization)	60
B.3	Derivation of the shifts of expectation values	60
B.4	Derivation of $ \Phi'_j\rangle$	60
B.5	Derivation of expectation values of complementary observables	61
B.6	Analysis of validity of expectation value expressions for strong interactions	62
B.6.1	Expectation Values of Final Pointer State	64
B.6.2	Calculation of Weak Value	64
B.6.3	Comparison of Expressions	65
B.7	Expectation values for Gaussian states	66
B.8	Derivation of the fit formula	67
	Acknowledgments	69

Contents	xi
Acknowledgments	69
List of figures	71
List of tables	71
Bibliography	75
Declaration of Authorship	82

Chapter 1

Introduction

Quantum mechanics is a fundamental theory in physics, which enabled to explain phenomena on smallest scales of the physical world, for which classical physics failed. Although it proved to be a very powerful theory, several problems with respect to its physical interpretation remain, especially concerning the postulated collapse of the wavefunction [Schlosshauer05, Schlosshauer13].

Almost 30 years ago, Aharonov, Albert, and Vaidman proposed a particular approach, namely the weak value concept, which avoids the consequences of the full collapse in the description of a measurement by considering only a weak measurement in a pre- and postselected system. It is based on the time-symmetric theory of quantum mechanics, which was presented about 20 years earlier by Aharonov, Bergmann, and Lebowitz [Aharonov64]. Since its debut, the physical meaning and significance of the weak value was discussed controversially [Duck89, Leggett89, Peres89] and there is still an ongoing debate [Aharonov02, Sokolovski13, Svensson13, Svensson14, Sokolovski16]. Over the years the focus changed from the weak value as a merely theoretical construct, utilized for arguments in the debate of paradoxes, to an experimental tool [Dressel14], as underlined by the ongoing emergence of publications [Martínez-Rincón17, Qiu17, Chen18, Singh18]. Especially the technique of the weak value amplification became successful as it allowed to observe weak effects as the Spin Hall effect of light [Hosten08]. Although many of the recent publications are about the experimental realization of weak value amplification, there are still papers emerging concerning fundamentals of the weak value, e.g., [Vaidman17]. The investigation of the properties of weak values and their applications is in the very same direction of research and is presented of almost the same group of authors in [Dziewior18] and in this thesis. The main work of the thesis was the experimental support for the demonstration of the theoretical concept, which was introduced and developed primarily in [Dziewior18].

While, usually, the weak value concept is considered only for a single

weak measurement, in this thesis the concept is extended to several interactions with various pointers and moreover considered for interactions of finite strength. By doing so, a modified weak value formula and a new property of the weak value is found, namely the universality property of the weak value. This property manifests as a universal modification of the shift in the expectation values of the various pointer systems, which was directly observed in a Mach-Zehnder interferometer. Furthermore, an alignment technique for interferometers is presented, which is based on considering the misalignment as an interaction of position and momentum, and which has been motivated by the newly introduced universality property.

The thesis is structured in the following way: In chapter 2 some fundamental concepts are described, which are important for the theoretical understanding of the thesis. The experimental framework is shown and explained in chapter 3. On this theoretical and experimental basis the weak value is investigated theoretically and experimentally and its universality property is derived in chapter 4. In chapter 5 the alignment technique is presented. After a summary and an outlook of this work, additional information about the setup and relevant mathematical calculations are given in the appendix.

Chapter 2

Fundamental principles

2.1 Quantum measurements

Quantum measurements are a subtle and important issue in quantum mechanics. One special property of quantum mechanics is the non-classical behavior of the measurement process. Contrary to classical mechanics, where measurements solely read off values, which exists independently of the measurement, in quantum mechanics a backaction from the measurement process is observable. Moreover, there is still no consensus about the interpretation of measurements in quantum mechanics. Therefore it is even more necessary to give a mathematical description of the measurement process, which is done in the following sections.

2.1.1 Projective measurements

In quantum mechanics a physical property is described by a Hermitian operator $\hat{\mathbf{A}}$. According to the *spectral theorem* for discrete, degenerate eigenvalues it can be expressed by

$$\hat{\mathbf{A}} = \sum_j a_j \hat{\mathbf{P}}_j, \quad (2.1)$$

with $\hat{\mathbf{P}}_j$ as the projector onto the subspace of eigenstates with the corresponding eigenvalue a_j . In his book PRINCIPLES OF QUANTUM MECHANICS Dirac wrote about measurements [Dirac58]:

A measurement always causes the system to jump into an eigenstate of the dynamical variable that is being measured, the eigenvalue of this eigenstate belongs to being equal to the result of the measurement.

A mathematical formulation of this statement is the following. Let the system be in the initial state ρ and further assume that its free Hamiltonian

is negligible. Then after the measurement of the dynamical variable $\hat{\mathbf{A}}$, the probability for a particular eigenvalue a_j is given by

$$\text{Prob}(a_j) = \text{Tr}(\rho \hat{\mathbf{P}}_j). \quad (2.2)$$

The state of the system will afterwards be

$$\rho_j = \frac{\hat{\mathbf{P}}_j \rho \hat{\mathbf{P}}_j}{\text{Tr}(\rho \hat{\mathbf{P}}_j)}. \quad (2.3)$$

This projection onto a subspace of the eigenstates is known as the *wave-function collapse* or *projection postulate*.

2.1.2 Generalization of the projection postulate

The projection postulate can be generalized in terms of *measurement operators* $\hat{\mathbf{M}}_m$, where m refers to the different outcomes of the measurement. Notice that these are not necessarily eigenvalues of a Hermitian operator. The corresponding post measurement state is given by

$$\rho_m = \frac{\hat{\mathbf{M}}_m \rho \hat{\mathbf{M}}_m^\dagger}{\text{Tr}(\rho \hat{\mathbf{M}}_m^\dagger \hat{\mathbf{M}}_m)}, \quad (2.4)$$

where the denominator is the probability for the measurement outcome m . A new operator can be now defined by means of $\hat{\mathbf{M}}_m$

$$\hat{\mathbf{E}}_m = \hat{\mathbf{M}}_m^\dagger \hat{\mathbf{M}}_m \quad (2.5)$$

which is called *probability operator* or *effect operator*. $\hat{\mathbf{E}}_m$ is Hermitian and has non-negative eigenvalues. The set of all effects satisfies

$$\sum_m \hat{\mathbf{E}}_m = \mathbb{1}_S, \quad (2.6)$$

where $\mathbb{1}_S$ is the identity operator of the system. This completeness condition can be derived from the probability relation $\sum_m \text{Prob}(m) = 1$ and the calculation of the probability

$$\text{Prob}(m) = \text{Tr}(\rho \hat{\mathbf{E}}_m). \quad (2.7)$$

The set of effects $\hat{\mathbf{E}}_m$ is called the *Positive-Operator Valued Measure (POVM)*. This mathematical tool is in particular useful if the system after the measurement is of little interest and the main focus lies on the probability of a measurement. It allows to account for more complicated measurement operations than simply the projection into eigenspaces of an observable. Furthermore this general formalism can be also applied to weak measurements.

2.1.3 Von Neumann measurement model

According to [Wiseman09] the above descriptions (sec. 2.1.1 and 2.1.2) of measurements are inadequate. As the system is not directly accessible, its effects on the environment, hence the interaction with the measurement apparatus are detected. Von Neumann developed a dynamical description of quantum measurements, which includes the measurement apparatus as a second quantum system, namely the *pointer* [Wiseman09], as depicted in fig. 2.1. With $|\Psi_I\rangle$ as the initial state of the system and $|\Phi_I\rangle$ as initial state

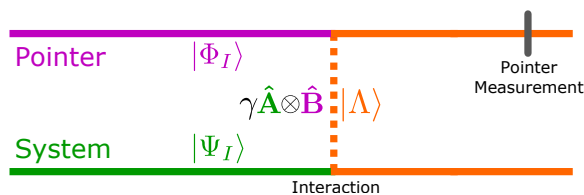


Figure 2.1: **Von Neumann measurement model:** The uncorrelated system $|\Psi_I\rangle$ and pointer $|\Phi_I\rangle$ couple during the measurement according to $\gamma \hat{A} \otimes \hat{B}$ and become correlated in the final state $|\Lambda\rangle$. Afterwards a projective measurement on the pointer is performed to obtain information about the system.

of the pointer we obtain for the composite initial state

$$|I\rangle = |\Psi_I\rangle \otimes |\Phi_I\rangle \quad (2.8)$$

$$= |\Psi_I\rangle |\Phi_I\rangle, \quad (2.9)$$

which is separable. For the further work, the shorthand notation of eq. (2.9) instead of eq. (2.8) for tensor products of states is used. For measuring \hat{A} , the system and the pointer couple according to the Hamiltonian

$$\hat{H} = \gamma \hat{A} \otimes \hat{B}, \quad (2.10)$$

where γ is the instantaneous coupling rate, which is nonzero only during the coupling time, and \hat{B} denotes the operator acting on the pointer, also called *indicator* [Kofman12]. After the coupling the system and the pointer are in general entangled in the final state $|\Lambda\rangle$

$$|\Lambda\rangle = \hat{U}|I\rangle = \hat{U}|\Psi_I\rangle|\Phi_I\rangle, \quad (2.11)$$

with

$$\hat{U} = \exp\left(-i\Gamma \hat{A} \otimes \hat{B}\right) \quad (2.12)$$

as the unitary evolution operator and $\Gamma = \gamma\tau$ as the coupling strength, where τ is the coupling time. Here and in the rest of the thesis we set $\hbar = 1$. A final measurement of the pointer yields information about the system.

Calculation of pointer expectation value

To calculate the pointer deviation after the measurement let us first calculate the final state. By assuming a discrete, degenerate observable $\hat{\mathbf{A}}$ (eq. (2.1)) we can write the initial system state as $|\Psi_I\rangle = \sum_n c_n |a_n\rangle$. Inserting this in equation (2.11) with $\hat{\mathbf{P}}_j = |a_j\rangle\langle a_j|$ we get for the final state

$$|\Lambda\rangle = e^{-i\Gamma \sum_j a_j \hat{\mathbf{P}}_j \otimes \hat{\mathbf{B}}} \sum_n c_n |a_n\rangle |\Phi_I\rangle \quad (2.13)$$

$$= \sum_j c_j |a_j\rangle e^{-i\Gamma a_j \hat{\mathbf{B}}} |\Phi_I\rangle. \quad (2.14)$$

As the system is not considered in the following, we take the partial trace over it and get the reduced density matrix for our pointer

$$\rho_\Phi = \text{Tr}_\Psi (|\Lambda\rangle\langle\Lambda|) \quad (2.15)$$

$$= \sum_j |c_j|^2 e^{-i\Gamma a_j \hat{\mathbf{B}}} |\Phi_I\rangle\langle\Phi_I| e^{i\Gamma a_j \hat{\mathbf{B}}}. \quad (2.16)$$

The expectation value of any observable $\hat{\mathbf{C}}$ of the pointer can simply be calculated by

$$\langle\hat{\mathbf{C}}\rangle = \text{Tr}(\rho_\Phi \hat{\mathbf{C}}). \quad (2.17)$$

For experiments presented later we look on the indicator $\hat{\mathbf{B}}$ and its canonically conjugate $\hat{\mathbf{C}}$. In the case of a continuous spatial pointer we have $\hat{\mathbf{B}} = \hat{\mathbf{p}}$ and $\hat{\mathbf{C}} = \hat{\mathbf{x}}$. Then we obtain for the expectation value

$$\langle\hat{\mathbf{x}}\rangle = \text{Tr} \left(\sum_j |c_j|^2 e^{-i\Gamma a_j \hat{\mathbf{p}}} |\Phi_I\rangle\langle\Phi_I| e^{i\Gamma a_j \hat{\mathbf{p}}} \hat{\mathbf{x}} \right) \quad (2.18)$$

$$= \sum_j |c_j|^2 \left(\text{Tr} \left(|\Phi_I\rangle\langle\Phi_I| e^{i\Gamma a_j \hat{\mathbf{p}}} \hat{\mathbf{x}} e^{-i\Gamma a_j \hat{\mathbf{p}}} \right) + \text{Tr} \left(|\Phi_I\rangle\langle\Phi_I| e^{i\Gamma a_j \hat{\mathbf{p}}} (-i\Gamma a_j) e^{-i\Gamma a_j \hat{\mathbf{p}}} \right) \right) \quad (2.19)$$

$$= \sum_j |c_j|^2 (\langle\hat{\mathbf{x}}\rangle_I + \Gamma a_j) \quad (2.20)$$

$$= \langle\hat{\mathbf{x}}\rangle_I + \Gamma \langle\hat{\mathbf{A}}\rangle. \quad (2.21)$$

From line (2.18) to (2.19) we used the commutation relation

$$[\hat{\mathbf{x}}_i, G(\hat{\mathbf{p}})] = i \partial G(\hat{\mathbf{p}}) / \partial \hat{\mathbf{p}}_i. \quad (2.22)$$

Considering eq. (2.20) the final pointer state can be written for non-degenerate eigenvalues as a shifted wavefunction $\langle x | \Phi_F \rangle = \Phi_I(x - \Gamma a_j)$. The coupling is sufficiently strong if

$$|\Gamma|(\delta a) \gg \Delta x \quad (2.23)$$

holds, with δa as the minimal distance between the different eigenvalues and Δx as the uncertainty of x of the initial pointer state. In this case, the components of the pointer wavefunction for different eigenvalues do not overlap and we have a projective measurement of $\hat{\mathbf{A}}$. If this condition is not satisfied, i.e., a not strong the coupling Γ , we call it a *non-ideal measurement*. Furthermore, if the system state remains nearly unchanged, it is called a *weak measurement*. Note that the pointer change (eq. (2.21)) in this case is smaller than the pointer uncertainty.

2.2 Two-state vector formalism

In classical physics the properties of an isolated system can be determined for all past and future times if its state and Hamiltonian are known for one moment in time. This determinism is in contrast to standard quantum mechanics, where the evolution is *non-deterministic* due to measurements. Because of a fundamental complementarity in quantum mechanics only a fraction of observables can be measured with arbitrarily high precision at the same time at on a single system. This probabilistic behavior makes the standard quantum theory *time-asymmetric*. Indeed there are few symmetrized approaches, e.g. [Aharonov64, Griffiths84, Oreshkov15]. The first one was provided by Aharonov, Bergmann and Lebowitz (ABL) already in the early 70's. According to them, a complete description of a system at time t is achieved by the *two-state vector*

$$\langle \Psi_F | \Psi_I \rangle, \quad (2.24)$$

where $|\Psi_I\rangle$ denotes the state defined by the measurements in the past relative to time t and $\langle \Psi_F|$ denotes a backward evolving state defined by measurements after time t . The authors of [Aharonov64] claim that this *Two-State Vector Formalism (TSVF)* then yields maximal information how the system affects others, especially measurement devices, at time t [Aharonov08]. But indeed, this is a very controversially discussed statement.

2.2.1 Measurements on pre- and postselected systems

To examine TSVF experimentally, ABL proposed measurements on *pre- and postselected systems (PPS)*, schematically depicted in figure 2.2. The preparation of an ensemble in the same initial state $|\Psi_I\rangle$ is called *preselection*. Considering only the system, on each identical copy of the ensemble a measurement of the observable $\hat{\mathbf{A}}$ is performed (indicated in fig. 2.2 by thin box with arrow), which can be either weak or strong. The *postselection* is done by means of a projective measurement of an observable $\hat{\mathbf{F}}$ and subsequent selection on one of the orthogonal states $|\Psi_{F,1}\rangle$, $|\Psi_{F,2}\rangle$, etc. Hence a PPS is defined by a certain $|\Psi_I\rangle$ and a certain $|\Psi_F\rangle$ of the system, where $|\Psi_F\rangle$

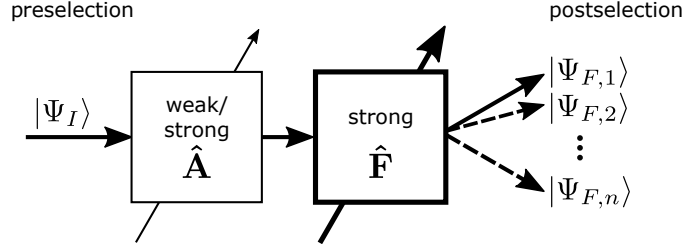


Figure 2.2: **Scheme of pre- and postselected measurement:** This scheme only considers the pre- and postsystem (PPS), not the pointer. An ensemble prepared in the system state $|\Psi_I\rangle$ is called *preselection*. A weak/strong measurement of \hat{A} on several copies is performed. Afterwards, for each copy, a projective measurement of \hat{F} is conducted with subsequent selection on certain eigenstate $|\Psi_{F,1}\rangle, |\Psi_{F,2}\rangle$, etc. which is called *postselection*. Adopted from [Kofman12].

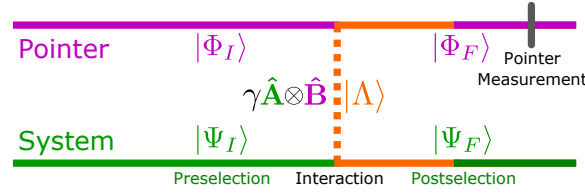


Figure 2.3: **Von Neumann scheme for PPS measurement:** Before the postselection, the description of the measurement process is the same as in the standard von Neumann measurement model. After the postselection on a certain system state $|\Psi_F\rangle$, the final pointer state $|\Phi_F\rangle$ also changes due to entanglement between system and pointer.

represents one of the final states $|\Psi_{F,1}\rangle, |\Psi_{F,2}\rangle$, etc.

When the PPS measurement is conducted via a von Neumann scheme (fig. 2.3), the effect on the final state of the pointer $|\Phi_F\rangle$ becomes

$$|\Phi_F\rangle = \langle \Psi_F | \Lambda \rangle = \langle \Psi_F | \left(\hat{U} |\Psi_I\rangle |\Phi_I\rangle \right) \quad (2.25)$$

$$= \langle \Psi_F | \left(\exp \left(-i\Gamma \hat{A} \otimes \hat{p} \right) |\Psi_I\rangle |\Phi_I\rangle \right) \quad (2.26)$$

$$= \mathcal{N} \langle \Psi_F | \Psi_I \rangle \sum_n \frac{(-i)^n}{n!} \Gamma^n \frac{\langle \Psi_F | \hat{A}^n | \Psi_I \rangle}{\langle \Psi_F | \Psi_I \rangle} \hat{p}^n |\Phi_I\rangle, \quad (2.27)$$

where \mathcal{N} is the normalization factor and using $|\Lambda\rangle$ from eq. (2.11). Eq. (2.27) is the Taylor expansion of the exponential operator. Compared to the standard measurements, PPS measurements exhibit some very special features, which will be discussed below.

2.2.2 The weak value

In this work, the TSVF is of special interest in the context of weak measurements. A simple standard approach to evaluate weak PPS measurements is to approximate eq. (2.27) to first order in Γ [Aharonov88, Aharonov90, Kofman12]

$$|\Phi_F\rangle \approx \mathcal{N}' \langle \Psi_F | \Psi_I \rangle \left(1 - i\Gamma \frac{\langle \Psi_F | \hat{\mathbf{A}} | \Psi_I \rangle}{\langle \Psi_F | \Psi_I \rangle} \hat{\mathbf{p}} \right) |\Phi_I\rangle \quad (2.28)$$

$$= \mathcal{N}' \langle \Psi_F | \Psi_I \rangle (1 - i\Gamma A_w \hat{\mathbf{p}}) |\Phi_I\rangle \quad (2.29)$$

$$\approx \mathcal{N}'' \langle \Psi_F | \Psi_I \rangle \exp(-i\Gamma A_w \hat{\mathbf{p}}) |\Phi_I\rangle, \quad (2.30)$$

where the different \mathcal{N}' and \mathcal{N}'' denote the corresponding normalization factors. From eq. (2.28) to eq. (2.29) the definition

$$A_w \equiv \frac{\langle \Psi_F | \hat{\mathbf{A}} | \Psi_I \rangle}{\langle \Psi_F | \Psi_I \rangle}, \quad (2.31)$$

was used, which is namely the *weak value* of $\hat{\mathbf{A}}$. It was first introduced by Aharonov, Albert and Vaidman (AAV) as the measurement outcome of a weak measurement on a PPS ([Aharonov88]). In the linear response regime, which is the most studied regime for weak values, the weak regime is bounded by

$$|\Gamma A_w| \Delta p \ll 1, \quad (2.32)$$

with Δp as the uncertainty of the indicator observable of the initial pointer state [Kofman12]. As an expectation value, the weak value can be measured only with certain accuracy on an ensemble due to the weakness of each measurement [Aharonov08]. However, it differs from an expectation value of an observable in a standard measurement: First, the weak value can be complex and second, it can diverge if the overlap $|\langle \Psi_F | \Psi_I \rangle|$ tends to zero. This has several consequences for the final pointer shift, which is given by [Kofman12]

$$\begin{aligned} \mathcal{D}_F(x) &\equiv \langle \Phi_F | \hat{\mathbf{x}} | \Phi_F \rangle - \langle \Phi_I | \hat{\mathbf{x}} | \Phi_I \rangle \\ &\approx \Gamma \operatorname{Re}[A_w] \end{aligned} \quad (2.33)$$

$$\mathcal{D}_F(p) \approx 2\Gamma (\Delta p)^2 \operatorname{Im}[A_w], \quad (2.34)$$

for $\hat{\mathbf{x}}$ and $\hat{\mathbf{p}}$. Notice that in general the pointer shape can change due to postselection. The fact that the weak value can be far outside of the range of the eigenvalues is often used for one of the applications of weak values: The *weak value amplification*, see sec. 2.2.3. There are also other possible applications using the features of weak values. The fact, that in

general the weak value is complex, is used for example for *direct state tomography* [Lundeen11, Massar11, Zilberberg11, Lundeen12, Kobayashi14, Malik14]. Furthermore, weak values can be used for conditioned average calculations, which yield arguments for paradoxes like *Hardy's paradox* [Aharonov02, Lundeen09, Resch04, Yokota09] and the *Three-Box-Paradox* [Aharonov91, Ravon07].

2.2.3 Weak value amplification

Among the various properties of weak values the most useful one for many applications is that the bounds of expectation values can be overcome. Especially for high sensitivity metrology, which aims to examine small effects, the so called technique of *weak value amplification* is interesting. A famous example which used this technique was realized by Hosten and Kwiat to measure the *Spin Hall Effect of Light*. They managed to amplify this hardly measurable effect by four orders of magnitude [Hosten08]. Another popular example was done by Dixon et al. who measured beam deflections down to the order of femtoradians by means of a Sagnac interferometer. In this experiment amplification factors of more than 100 were achieved [Dixon09]. As already mentioned, eq. (2.33) and eq. (2.34) show that the pointer shift is directly related to the weak value A_w . Thus, by increasing A_w beyond the range of the eigenvalues the shift can be modified. The weak value A_w , and therefore the modification, can be either real positive, real negative, imaginary or complex. For the real positive case the pointer change (eq. (2.33)) is just amplified (or reduced) in the same direction compared to an shift induced by a measurement on an only preselected system. If A_w is negative, the amplification acts in the opposite direction compared to the interaction. In the case of a imaginary A_w eq. (2.33) would not yield any change. Instead, the shift will manifest in the conjugate variable $\hat{\mathbf{p}}$, as described by eq. (2.34). In general A_w is complex and therefore a combination of the mentioned cases. In the linear regime, the amplification \mathcal{A} is of the order of magnitude [Aharonov88], [Hosten08]

$$\mathcal{A} \sim |\langle \Psi_F | \Psi_I \rangle|^{-1}, \quad (2.35)$$

which is exactly the denominator in the definition of the weak value (eq. (2.31)). Note that this is the inverse of the overlap of the initial and final system state, and thus by choosing suitable pre- and postselected states for the system a large amplification factor can be achieved.

Let us consider the example presented in [Aharonov08], which is a modified version of the original idea presented in the paper HOW THE RESULT OF A MEASUREMENT OF A COMPONENT OF THE SPIN OF A SPIN-1/2 PARTICLE CAN TURN OUT TO BE 100 [Aharonov88]. For this purpose, let us assume a Stern-Gerlach experiment, with $|\uparrow_x\rangle$ as the preselected and $|\uparrow_y\rangle$ as the postselected state and a spatial Gaussian pointer. With eq. (2.31) and

$\hat{\sigma}_\xi = (\hat{\sigma}_x + \hat{\sigma}_y)/\sqrt{2}$ as the weak interaction in the $\hat{\xi}$ direction the weak value calculates to

$$(\sigma_\xi)_w = \frac{1}{\sqrt{2}} \frac{\langle \uparrow_y | (\hat{\sigma}_x + \hat{\sigma}_y) | \uparrow_x \rangle}{\langle \uparrow_y | \uparrow_x \rangle} = \sqrt{2}, \quad (2.36)$$

which is clearly outside of the range of expectation values of $[-1, +1]$. After a measurement according to the standard measurement model in fig. 2.1, the probability distribution on a detector with the spatial variable q is described by

$$\text{Prob}(q) \propto \cos^2(\pi/8) \cdot e^{-\frac{(q-1)^2}{(\Delta)^2}} + \sin^2(\pi/8) \cdot e^{-\frac{(q+1)^2}{(\Delta)^2}}, \quad (2.37)$$

in the eigenstates of $\hat{\sigma}_\xi$.

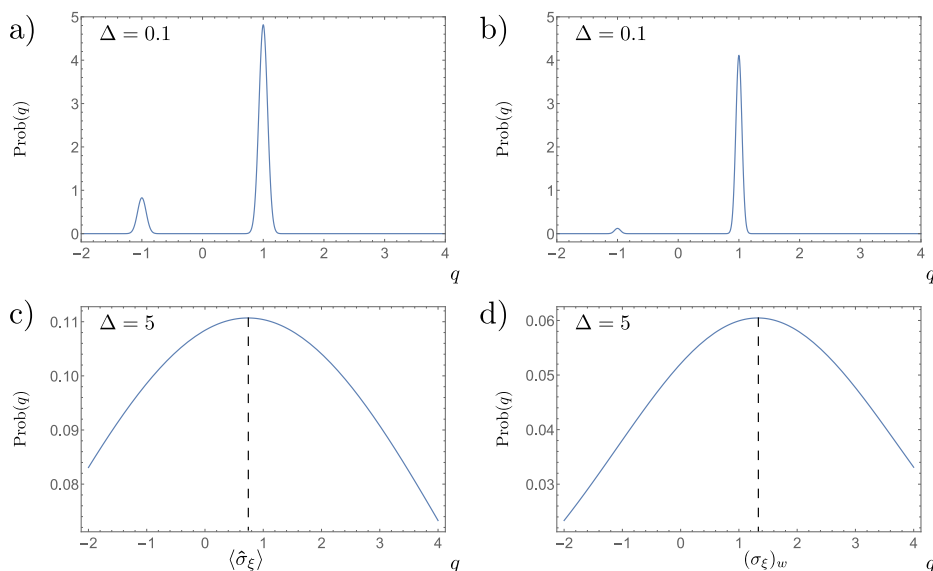


Figure 2.4: **Comparison standard measurement with PPS measurement:** The upper row shows probability distributions of a strong measurement a) in a standard way and b) in a PPS ensemble. Both have peaks located at the eigenvalues ± 1 . The lower row shows probability distributions for weak measurement, c) without postselection and d) for PPS. In c) the peak is located at expectation value $1/\sqrt{2}$ and in d) close to the weak value $\sqrt{2}$. Adapted from [Aharonov08].

The result for a standard strong measurement ($\Delta \ll 1$) is shown in fig. 2.4 a). There are two peaks with a certain width localized around the eigenvalues ± 1 .

For a weak measurement the width of the distribution is much larger than the shift ($\Delta \gg 1$), and only one peak is recognizable, located at the expectation value $\langle \uparrow_x | \hat{\sigma}_\xi | \uparrow_x \rangle = 1/\sqrt{2}$. When we now consider the measurement

with postselection on $|\uparrow_y\rangle$ (fig. 2.3), we obtain

$$\text{Prob}(q_F) \propto \left(\cos^2(\pi/8) \cdot e^{-\frac{(q-1)^2}{2(\Delta)^2}} - \sin^2(\pi/8) \cdot e^{-\frac{(q+1)^2}{2(\Delta)^2}} \right)^2 \quad (2.38)$$

as the probability distribution of the pointer. The result is depicted again for a strong measurement in fig. 2.4 b) and for a weak interaction in fig. 2.4 d) for a PPS. Different to the weak standard measurement the peak is no longer located at $\langle \hat{\sigma}_\xi \rangle = 1/\sqrt{2}$ but at the weak value $(\sigma_\xi)_w \approx \sqrt{2}$.

Advantages and limits of weak value amplification

In [Dressel14, Knee14] the advantages of the weak value amplification is discussed. For the weak value method only a fraction of the whole ensemble is needed, but it has similar sensitivity for the parameter estimation. This is an advantage in scenarios where the number of detectable particles is bounded, e.g., due to dead-time or saturation of the detector. Furthermore the rest of the ensemble can be redirected and used for another measurement. This technique amplifies the signal, so for a sufficiently large weak value the pointer shift can overcome technical noise.

The increasing popularity of weak values gave rise to the question whether it can be a superior method for parameter estimation. For instance, the authors in [Ferrie14, Knee14, Tanaka13] tried to find an answer to this question. By considering the Fisher information they concluded that this method will not outperform standard metrology strategies. One can also become aware about the limits of weak value amplification in a more intuitive way. As already mentioned, to determine the weak value with desired accuracy a certain number of particles is necessary. In the language of optical physics a certain number of photons is needed. When the weak value increases the detection probability decreases due to the small overlap of the initial and final state. This makes longer collection times necessary to get a sufficient precision. Thus, a larger amplification factor effectively keeps the signal to noise ratio constant ([Knee13, Dressel14, Ferrie14]). So in the end it is a question of resources whether the weak value amplification is useful or not.

Chapter 3

Experimental framework

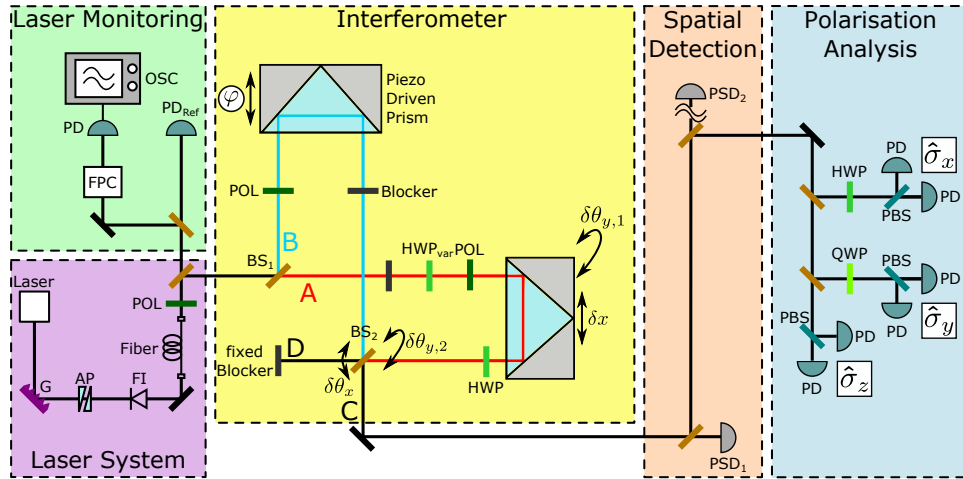


Figure 3.1: **Experimental setup:** In the *Laser System* the light is generated at 780 nm with the desired properties, which are monitored in the *Laser Monitoring* part. The core of the experimental framework is the *Interferometer* part, which consists of a folded Mach-Zehnder interferometer (MZI), in which the optical path length, the intensity ratio, the polarization and the spatial deviation in one arm relative to the other can be set. The *Spatial Detection* is done by means of two position sensing detectors (PSDs) at different distances along the propagation direction of the beam. In the *Polarization Analysis* the polarization is measured in the basis of $\hat{\sigma}_{x,y,z}$.

The performed experiments are based on novel theoretical insights discussed in chapter 4 and presented in [Dziewior18]. Therefore, the experimental framework is explained in this chapter, so that the following chapters can mainly focus on the theory and its connection to the measured results. In fig. 3.1 the experimental setup is shown. It is structured in five parts, namely the *Laser System*, the *Laser Monitoring*, the *Interferometer*, the

Spatial Detection, and the *Polarization Analysis*. For easier understanding these different parts are explained separately in the following sections. More details about the used optical components can be found in the appendix A.1.

3.1 The different experimental parts

3.1.1 Laser System

The employed temperature stabilized laser diode (LD) is frequency stabilized by the external-cavity technique in the Littrow configuration, which mainly consists of a collimating lens and a diffraction grating (G). The method of the external cavity allows for achieving a narrow wavelength spectrum and high tunability [Kneubühl08, Meschede09]. In the presented configuration diffracted light of first order is backreflected into the resonator, where it provides optical feedback. The diffraction of zeroth order is reflected as the output beam [Hecht87, Kneubühl08, Meschede09], which has a wavelength of about 780 nm. By means of an anamorphic prism pair (AP) the profile of the output beam, which is initially elliptical, is reshaped to a circle. After passing a Faraday isolator (FI), which prevents that light couples back to the laser, the light is spatially filtered by a single mode fiber. The emitted beam after the fiber coupler can be well characterized by the Rayleigh range z_R , which is correlated to the waist of the beam w_0 by $z_R = \pi w_0^2 / \lambda$. The Rayleigh range z_R as well as the position of the waist z_0 , which was subsequently defined as the origin in the propagation direction z , were determined by an optimization procedure ($z_R = 4.1$ m). Behind the fiber coupler, the beam is horizontally polarized with a polarizer (POL) and split up by a beam splitter (BS). The main part is sent to the interferometer and the residual part is used to monitor some laser properties.

3.1.2 Laser Monitoring

The output power P_{out} of the incident laser beam is recorded by a reference photo diode (PD_{ref}). The experimental data is normalized by P_{out} to cancel out laser fluctuations. Because of the disadvantage of mode-hopping in the given laser system configuration, the longitudinal mode of the laser is monitored by means of a photodiode behind a Fabry-Pérot cavity (FPC) whose signal is displayed on an oscilloscope (OSC). Due to the accidental wavelength change the monitoring is necessary to have knowledge about the laser beam which is directed to the experiment.

3.1.3 Interferometer

The core of the experiments performed in this thesis is a folded Mach-Zehnder-interferometer (MZI). It is realized by two balanced beam split-

ters and two retroreflecting prisms, with the latter mounted on translation stages. Each arm contains a beam blocker, which can be moved in and out of the beam as controlled by the computer, and a fixed H-polarizer (POL). By means of the motorized halfwave plate in front of the POL in arm A (HWP_{var}) the intensity ratio can be set to any desired value $I_A/I_B \lesssim 1$. With the motorized halfwave plate (HWP) behind the prism in arm A the initial polarization of horizontally polarized light $|H\rangle$ can be changed according to eq. (A.2). In combination with the fixed POL in each arm the relative polarization of arm A to arm B can be set. By tilting the second beam splitter BS_2 the beam of A with respect to B can be deflected in x - and y -direction, where the latter is perpendicular to the drawing plane. The translation stage of the prism in arm A is moved by a stepper motor in x -direction, furthermore it can be tilted in y -direction. With this configuration any desired displacement as well as angular deviation in x and y can be adjusted (for more details see section 3.2.2).

To set the relative phase between the two arms a translation stage in arm B moves the retroreflecting prism in beam direction. For the measurements it is periodically driven by a piezo, which changes the optical path length and thus the phase between the two arms.

For the subsequent analysis only the photons deflected behind the output port C are used.

3.1.4 Spatial Detection

The spatial detection is done with Position Sensing Detectors (PSD). The x position in millimeters is read out by the corresponding voltage V_x (the origin is located at the center of the PSD) according to

$$x = \frac{V_x}{V_{\text{sum}}} \cdot 5[\text{mm}], \quad (3.1)$$

(analogous for y), with V_{sum} denoting the sum voltage and 5 as the required conversion factor. More details about the behavior dependent on the sum voltage is given in the appendix A.2.2.

For the experiment described in chapter 4 it is crucial to determine simultaneously the relative position and angle of the beams. By placing the PSD in the waist of the Gaussian beam z_0 , only position shifts would be recorded, and for a placement in the far field only angular shifts would be measured. But in the real experimental setup neither the first nor the second case was given. Still it is possible to determine displacement and angle by means of two PSDs at different distances, as described in sec. 3.2.1.

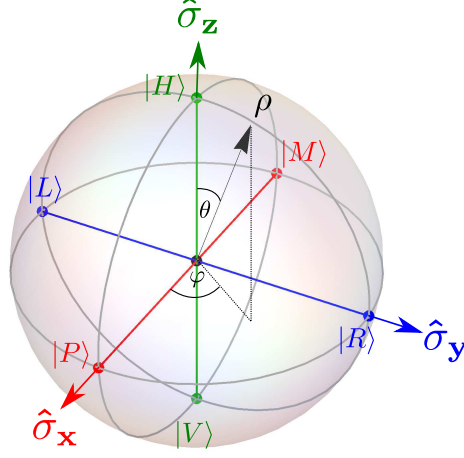


Figure 3.2: **Bloch sphere:** The polarization of a photon can be described as a two-level system. Therefore, it can be visualized in the Bloch sphere as a vector ρ , defined by the angles θ and φ . Horizontally $|H\rangle$ and vertically $|V\rangle$ polarized light are eigenstates of $\hat{\sigma}_z$ and thus located at the poles of the sphere. The x -axis corresponds to $\hat{\sigma}_x$ with diagonally $|P\rangle$ and antidiagonally $|M\rangle$ polarized light as eigenstates. Left $|L\rangle$ and right $|R\rangle$ circularly polarized light are eigenstates of $\hat{\sigma}_y$ and located at the poles of its direction.

3.1.5 Polarization Analysis

Every state of two-level system ρ , and thus also the polarization state of a photon, can be described by a density matrix parametrized as

$$\rho = \frac{1}{2} (\mathbb{1}_2 + \langle \hat{\sigma}_x \rangle \hat{\sigma}_x + \langle \hat{\sigma}_y \rangle \hat{\sigma}_y + \langle \hat{\sigma}_z \rangle \hat{\sigma}_z), \quad (3.2)$$

with $\mathbb{1}_2$ as the identity operator in two dimensions and $\hat{\sigma}_{x,y,z}$ as the Pauli matrices with the corresponding expectation values $\langle \sigma_{x,y,z} \rangle$. Horizontally $|H\rangle$ and vertically $|V\rangle$ polarized light are the eigenstates of $\hat{\sigma}_z$, diagonally $|P\rangle$ and antidiagonally $|M\rangle$ polarized light are eigenstates of $\hat{\sigma}_x$ and right $|R\rangle$ and left $|L\rangle$ circularly polarized light are the eigenstates of $\hat{\sigma}_y$. A pure polarization state ρ can be visualized using the Bloch sphere coordinates by

$$\rho = \begin{pmatrix} \cos^2 \frac{\theta}{2} & e^{-i\varphi} \cos \theta \sin \frac{\theta}{2} \\ e^{i\varphi} \cos \theta \sin \frac{\theta}{2} & \sin^2 \frac{\theta}{2} \end{pmatrix}, \quad (3.3)$$

where θ and φ are the rotation angles, as depicted in fig. 3.2.

This state can be determined by a polarization analysis (shown in fig. 3.1

blue box). Here the approach of a quantum state tomography is employed, i.e., determining a state ρ given by eq. (3.2), by measuring the set of incompatible observables $\hat{\sigma}_{x,y,z}$ and determining the probabilities of the different outcomes. The measurement of the probabilities is realized by a measurement of the normalized intensities in the different bases, e.g. for $\hat{\sigma}_z$

$$\langle \sigma_z \rangle = \text{Tr}(\rho|H\rangle\langle H|) - \text{Tr}(\rho|V\rangle\langle V|) \quad (3.4)$$

$$= \frac{I_{|H\rangle} - I_{|V\rangle}}{I_{|H\rangle} + I_{|V\rangle}}. \quad (3.5)$$

Because a polarizing beam splitter (PBS) always acts in the eigenbasis of $|H\rangle$ and $|V\rangle$, additional waveplates (half wave plate (HWP) and quarter wave plate (QWP)) are necessary to rotate into the desired measurement basis $\hat{\sigma}_x$ and $\hat{\sigma}_y$ respectively.

3.2 Geometrical considerations

The incident beams in the interferometer arms originate from a laser diode and a single mode fiber, thus are well described as Gaussian beams. However, if we are only interested at the center position along the propagation direction it is enough to consider them with ray optics.

3.2.1 Obtaining the spatial and angular displacement

As already mentioned, it is necessary to determine the spatial and angular deviation at the same time for the experiment presented in chapter 4. For the case that the PSDs are not located at the waist position of the beams z_0 or in the far field these deviations can not be recorded independently of each other. Still they can be determined by using both PSDs. In fig. 3.3

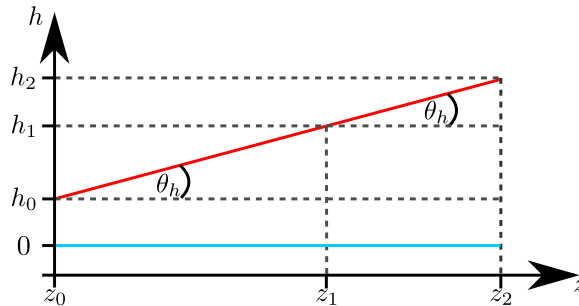


Figure 3.3: Geometrical scheme to derive angular and spatial deviation, i.e., θ_h and h_0 , between the beam of arm A (red) to that of arm B (blue) at the position of the waist z_0 by means of two PSDs located at different distances z_1 and z_2 with corresponding spatial deviations h_1 and h_2 .

the beam of arm B , which is directed along the z -axis, is taken as reference and therefore depicted as blue zero line at the height $h = 0$ on the PSD. The beam of arm A , represented as red line and also propagating in z -direction, has a different position h_0 and a different angle θ_h to the beam of arm B in the position of the waist z_0 , which was defined as the zero position along z . These deviations are given by

$$\theta_h = \arctan \left(\frac{h_2 - h_1}{z_2 - z_1} \right) \quad (3.6)$$

$$h_0 = h_1 - (z_1 - z_0) \cdot \tan \theta_h \quad (3.7)$$

$$= h_2 - (z_2 - z_0) \cdot \tan \theta_h, \quad (3.8)$$

with $z_1 = -0.24$ m and $z_2 = 5.27$ m as the z -positions of PSD₁ and PSD₂, respectively. The distance between both detectors was measured manually $z_2 - z_1 = (6.61 \pm 0.02)$ m.

3.2.2 Setting the spatial and angular displacement

For the experiment presented in chapter 5, it is crucial to know how to set a certain spatial and angular displacement in x - as well as in y -direction. For x the strategy is obvious. The spatial displacement δx can be set by moving the prism with the stepper motor and the angle $\delta\theta_x$ is set by tilting BS₂ in x . For the y -direction the spatial and angular displacement have to be set with two optical components, namely the prism in arm A and the beam splitter BS₂, which can only deflect the beam in y .

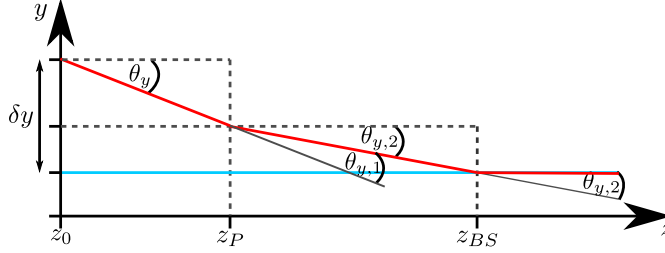


Figure 3.4: Geometrical considerations about how to set a displacement δy and an angle θ_y between the beam of arm A (red) to that of arm B (blue) at the waist position z_0 by tilting two components in arm A , i.e., $\theta_{y,1}$ at the prism located at z_P and $\theta_{y,2}$ at the BS₂ located at z_{BS} .

The blue line in fig. 3.4 depicts the beam of arm B , which is again taken as reference. The beam of arm A (red) has a certain spatial displacement δy and a certain angle θ_y to the beam of arm B at the position of the waist z_0 . Fig. 3.4 clarifies how to tilt the two components to overlap the beams of the different arms. The prism at z_P is rotated by about $\theta_{y,1}$ and the BS₂ at z_{BS} by about $\theta_{y,2}$ to obtain the desired displacement δy and angle

$\theta_y = \theta_{y,1} + \theta_{y,2}$. $\theta_{y,1}$ is chosen such that at z_{BS} only an angular deviation of $\theta_{y,2}$ is left. These rotation angles are given by

$$\theta_{y,1} = \theta_y - \arctan \left(\frac{\delta y}{z_{BS} - z_P} + \frac{z_0 - z_P}{z_{BS} - z_P} \tan \theta_y \right) \quad (3.9)$$

$$\theta_{y,2} = \theta_y - \theta_{y,1}. \quad (3.10)$$

Chapter 4

Universality of weak values

4.1 Introduction

The weak value is a key element of the two-state vector formalism (TSVF). Up to here it was considered with only one weak interaction in a pre- and postselected ensemble. But every (quantum) particle can experience different interactions due to its various properties, e.g. charge, mass, magnetic moment, etc., and of course also the same type of interaction multiple times. This gives rise to the question: Is the weak value concept still valid for multiple interactions? If so, in which way are the pointers affected?

In this section these questions are investigated in the framework of a Mach-Zehnder interferometer (MZI) with several interactions in only one arm. For this purpose a new description about the influence of interactions on external systems, i.e., pointers, is introduced. In the first instance the concept is derived for a system consisting of only one path, in which the interactions are located. Next, this approach is applied to one arm of the interferometer, whereas in the other arm no interactions occur. Ultimately, in this context the effect of various interactions on external systems can be evaluated theoretically and experimentally. The experimental demonstration was done by introducing three different couplings in one arm of the interferometer and recording the pointer shift. Furthermore, a modified formula for the weak value of the projection operator is found by considering interactions of finite strength. Its parameter dependency is also tested experimentally.

4.2 Theoretical considerations

To investigate various interactions in the context of the weak value concept, at first we want to consider the effect of them on *external systems*, i.e., pointers, in a single-path system. A scheme of this scenario is depicted in fig. 4.1 a). The initial state of all external systems together is denoted as $|\Phi\rangle$. In general, every successive interaction with a passing quantum particle

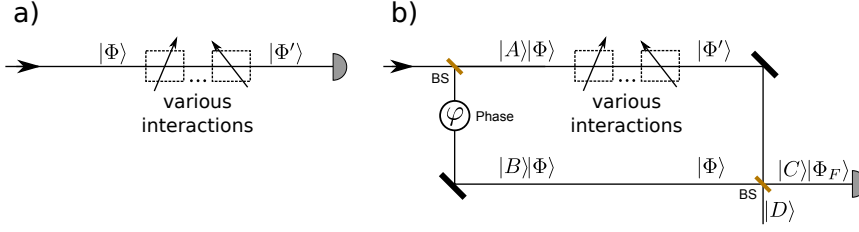


Figure 4.1: **Comparison of the effect of various interactions in a single-path system and in a MZI:** a) The quantum particle interacts with external systems in the path, which are all together initially in state $|\Phi\rangle$ and after the coupling in state $|\Phi'\rangle$. b) The scenario of a) is applied to arm A , whereas in arm B no interactions occur. The phase between the two arms can be shifted, which is indicated by φ in arm B . The effect on the external systems is detected in a) at the end of the path and in b) at the output port C , with the external system after the postselection in state $|\Phi_F\rangle$. Adapted from [Dziewior18].

which is illustrated as a dashed box with arrow, has an effect on the respective external system. Hence, after all interactions their state has changed to

$$|\Phi'\rangle \equiv \eta \left(|\Phi\rangle + \epsilon |\Phi^\perp\rangle \right), \quad (4.1)$$

with $|\Phi^\perp\rangle$ as some orthogonal component to $|\Phi\rangle$. Without loss of generality the phase of $|\Phi^\perp\rangle$ is chosen such that $\epsilon > 0$ (see for details B.4). By neglecting the global phase and by considering the normalization condition for $|\Phi'\rangle$ the overlap η of $|\Phi\rangle$ and $|\Phi'\rangle$ can be determined to

$$\eta = \langle \Phi' | \Phi \rangle = \frac{1}{\sqrt{1 + \epsilon^2}}. \quad (4.2)$$

For a weak coupling, i.e., $\epsilon \ll 1$ and thus $\eta = 1 + \mathcal{O}(\epsilon^2)$, eq. (4.1) can be approximated to

$$|\Phi'\rangle = |\Phi\rangle + \epsilon |\Phi^\perp\rangle + \mathcal{O}(\epsilon^2). \quad (4.3)$$

So the effect of interactions on the external systems manifests as some orthogonal component $|\Phi_\perp\rangle$ with respect to the initial state.

Now this description is applied for one arm of a Mach-Zehnder interferometer (MZI), as it is depicted in fig. 4.1 b). The other arm is considered to have no interactions, hence the state of the external systems remains $|\Phi\rangle$. We assume the first beam splitter (BS) to be unbalanced and thus obtain for the preselected system state

$$|\Psi_I\rangle = \cos \alpha |A\rangle + e^{i\varphi} \sin \alpha |B\rangle, \quad (4.4)$$

i.e., a superposition of arm A and B with α and φ as real parameters. The phase φ between arm A and B and can be varied as described in section 3.1.3, which is illustrated by φ in arm B (see fig. 4.1). After the interaction in arm A and before the overlap at the output beam splitter the composite state is given by

$$|\Lambda\rangle = \cos\alpha|A\rangle|\Phi'\rangle + \sin\alpha e^{i\varphi}|B\rangle|\Phi\rangle. \quad (4.5)$$

These considerations are necessary to derive in the next step the weak value and the pointer shifts for several interactions and/or several external systems of an interferometric PPS.

4.2.1 Calculation of the weak value

Now we want to derive the weak value in an interferometric PPS, as depicted in fig. 4.1. As illustrated, all interactions are located in arm A , hence the weak value is calculated for the projection operator onto this arm $\hat{\mathbf{P}}_A = |A\rangle\langle A|$. For an unbalanced input beam splitter followed by a phase shifter, the preselected state is given by eq. (4.4). In principle the second BS can also be unbalanced but for simplicity it is considered as a balanced one. The postselection corresponds to confine oneself to quantum particles arriving in output port C , hence the postselected state is given by

$$|\Psi_F\rangle = |C\rangle = \frac{1}{\sqrt{2}}(|A\rangle + |B\rangle), \quad (4.6)$$

which is described in appendix A.1.4. By using the definition of eq. (2.31) the weak value is calculated to

$$(P_A)_w = \frac{\langle\Psi_F|\hat{\mathbf{P}}_A|\Psi_I\rangle}{\langle\Psi_F|\Psi_I\rangle} \quad (4.7)$$

$$= \frac{(\langle A| + \langle B|)|A\rangle\langle A|(\cos\alpha|A\rangle + e^{i\varphi}\sin\alpha|B\rangle)}{(\langle A| + \langle B|)(\cos\alpha|A\rangle + e^{i\varphi}\sin\alpha|B\rangle)} \quad (4.8)$$

$$= \frac{1}{1 + \tan\alpha e^{i\varphi}}, \quad (4.9)$$

with

$$\tan\alpha = \sqrt{\frac{I_B}{I_A}}, \quad (4.10)$$

where I_A and I_B are the intensities of the respective beams in arms A and B . Notice that formula (4.9) is only valid for an ideal interferometer with very weak coupling, i.e., the system state remains effectively unchanged during the interaction.

Calculation for finite interaction strength

As already described in section 2.2 in the TSVF the state of the system is defined via the weak value for a certain moment in time t . Hence, for the evaluation of the forward and backward evolving system state all changes until time t have to be taken into account, which are assumed to be negligible in eq. (4.9). For the case that such changes are no longer negligible, the system state experiences a loss of coherence. This can happen due to imperfections of optical components and finite interaction strengths, in which the system becomes entangled with the pointer state. Thus, the introduced preselected state (eq. (4.4)) is only valid directly after the first BS and the postselected state (eq. (4.6)) is only valid directly before the second BS. Therefore the formula (4.9) is not suitable for a scenario in which coherence losses occur. A proper description can be achieved by taking into account the effective changes due to the interactions of the system with external systems eq. (4.1). Furthermore, all imperfections are also considered as additional interactions which also contribute to $|\Phi'\rangle$.

Now, in the framework of the MZI of fig. 4.1 in general the forward and backward evolving system states change between the first and the second BS, whereas the weak value $(P_A)_w$ remains constant in time. This is the case if all interaction operators commute with each other and with the spatial projection operator \hat{P}_A . This fact provides the opportunity to choose the moment in time at which the weak value is calculated, given that the forward and backward evolving state are evaluated at this time. For convenience the moment just before the second BS is chosen, thus the postselected state is still described by eq. (4.6). By taking the partial trace of eq. (4.5) over the external systems one obtains the preselected density matrix in the basis of $\{|A\rangle, |B\rangle\}$

$$\rho_I = \begin{pmatrix} \cos^2 \alpha & \cos \alpha \sin \alpha e^{-i\varphi\eta} \\ \cos \alpha \sin \alpha e^{i\varphi\eta} & \sin^2 \alpha \end{pmatrix}, \quad (4.11)$$

see appendix B.1. These states of the interferometric PPS can now be inserted in the generalized expression for the weak value of the operator \hat{A} from [Vaidman17]

$$A_w = \frac{\text{Tr}(\rho_F \hat{A} \rho_I)}{\text{Tr}(\rho_F \rho_I)}, \quad (4.12)$$

which simplifies due to the purity of the postselected state $\rho_F = |\Phi_F\rangle\langle\Phi_F|$. Notice that the formula (4.12) is only applicable before or after all interactions. In between it is only suitable if the forward and backward evolving states are entangled with different external systems. More details about the expression (4.12) can be found in [Vaidman17]. Finally the weak value can

be calculated to

$$(P_A)_w = \frac{\text{Tr}(|\Psi_F\rangle\langle\Psi_F|\hat{\mathbf{P}}_A\rho_I)}{\text{Tr}(|\Psi_F\rangle\langle\Psi_F|\rho_I)} \quad (4.13)$$

$$= \frac{1 + \tan\alpha\eta e^{-i\varphi}}{1 + \tan^2\alpha + 2\tan\alpha\eta\cos\varphi}, \quad (4.14)$$

which will be denoted here and in the following as *modified weak value*. The modified weak value (eq. (4.14)) is a function of the overlap η , the square root of the intensity ratio $\tan\alpha$ and the phase between the two arms φ . This parameter dependence is depicted in fig. 4.2 (placed at the end of this section) for chosen values of η in the real and imaginary part respectively. For a perfect overlap ($\eta = 1$) singularities appear, which turn into finite extrema as soon as $\eta < 1$. The smaller the overlap η the smaller the maximally achievable amplification factor becomes and therefore the more these extrema smear out. For a fixed intensity ratio $\tan\alpha$ the real part is a symmetric function of the phase φ , whereas the imaginary part is an antisymmetric one. This behavior was experimentally observed for $\eta = 0.990$ and $\tan\alpha = 1.33$ (see sec. 4.3.2), which is indicated by the horizontal violet line. For the fixed parameter $\varphi = \pi$ the real part exhibits an antisymmetric behavior as soon as $\eta < 1$ with respect to the rescaled parameter α . All of these curves intersect at the value 0.5 for $\tan\alpha = 1$, which is exhibited in fig. 4.6. This dependency was investigated in sec. 4.3.3, which is indicated by the vertical black lines.

4.2.2 External systems in interferometric PPS

In this section the effect of several, also different interactions on postselected external systems is investigated. The state of the postselected pointer can be determined according to eq. (2.25)

$$|\Phi_F\rangle = \mathcal{N}\langle\Psi_F|\Lambda\rangle \quad (4.15)$$

$$= \mathcal{N}\left(|\Phi\rangle + \epsilon\frac{\eta}{\eta + \tan\alpha e^{i\varphi}}|\Phi^\perp\rangle\right), \quad (4.16)$$

with the corresponding calculation in the appendix B.2. Again expanding the formula in terms of ϵ and recalling the formula for the modified weak value (eq. (4.14)) equation (4.16) can be rewritten as

$$|\Phi_F\rangle = |\Phi\rangle + \epsilon(P_A)_w|\Phi^\perp\rangle + \mathcal{O}(\epsilon^2). \quad (4.17)$$

A comparison with eq. (4.3) shows that the effect of the interactions are amplified in a universal manner, with the weak value of the projection operator $(P_A)_w$.

Considering various independent external systems

Now, let us assume a finite ϵ , which is constituted by all introduced interactions, in the ansatz of eq. (4.1). For this case the naive approach of inserting eq. (4.14) into eq. (4.17) would not give the correct prediction [Dziewior18]. We want to examine if still a statement can be made about the change of effects, which occurred due to weak interactions. For this purpose the external systems are considered individually.

The initial state of several external systems $|\Phi\rangle$ can be expressed as the product state

$$|\Phi\rangle = \bigotimes_j |\Phi_j\rangle \quad (4.18)$$

if the various systems, denoted by the index j , are independent of each other. With this ansatz eq. (4.1) can be rewritten as

$$|\Phi'\rangle = \bigotimes_j \eta_j \left(|\Phi_j\rangle + \epsilon_j |\Phi_j^\perp\rangle \right). \quad (4.19)$$

Given this interaction, the pure state of the j -th system in arm A evolves to

$$\rho'_j = \begin{pmatrix} 1 & \epsilon_j \\ \epsilon_j & 0 \end{pmatrix} + \mathcal{O}(\epsilon_j^2) \quad (4.20)$$

expressed in the basis of $\{|\Phi_j\rangle, |\Phi_j^\perp\rangle\}$ in analogy to eq. (4.19). The pointer state (eq. (4.20)) changes after the postselection to

$$(\rho_j)_F = \begin{pmatrix} 1 & (P_A)_w^* \epsilon_j \\ (P_A)_w \epsilon_j & 0 \end{pmatrix} + \mathcal{O}(\epsilon_j^2). \quad (4.21)$$

This equation shows that the off-diagonal elements, which are related to the orthogonal components of the single pointer in first order of ϵ_j , are affected by the weak value. So indeed, the modified weak value is still the correct modification factor for effects on the individual external systems, if the interaction with this particular system was weak and the effect of $\mathcal{O}(\epsilon_j^2)$ can be neglected ($\epsilon_j \ll 1$).

4.2.3 New insights in the change of expectation values

Up to here, the introduced concept, which describes the effect of interactions on external systems as an additional orthogonal component (c.f. eq. (4.1)), has been considered in an abstract manner. Experimentally, this additional orthogonal component in the state of the pointers manifests as shift in the expectation values of the observables of the external systems. If the external systems are all along one path (fig. 4.1 a)), the change of the expectation

value of the observable \hat{C} can be determined by

$$\mathcal{D}(C) \equiv \langle \Phi' | \hat{C} | \Phi' \rangle - \langle \Phi | \hat{C} | \Phi \rangle \quad (4.22)$$

$$= 2\epsilon \operatorname{Re} \left[\langle \Phi | \hat{C} | \Phi^\perp \rangle \right] + \mathcal{O}(\epsilon^2), \quad (4.23)$$

using the derivation given in B.3. In a pre- and postselected system (fig. 4.1 b)) we obtain with an analogous calculation

$$\mathcal{D}_F(C) = \langle \Phi_F | \hat{C} | \Phi_F \rangle - \langle \Phi | \hat{C} | \Phi \rangle \quad (4.24)$$

$$= 2\epsilon \operatorname{Re} \left[\langle \Phi | \hat{C} | \Phi^\perp \rangle (P_A)_w \right] + \mathcal{O}(\epsilon^2). \quad (4.25)$$

The formula (4.25) is the most important formula of this thesis. It shows that the effect observable after interactions on any and every external system, that was coupled weakly to the quantum particle exiting the interferometer in, e.g., arm C is modified in a universal manner. We denote this fundamental property as the *universality* of the weak value, here of the projection operator $(P_A)_w$. This insight has been found recently in [Dziewior18].

As already mentioned in section 2.2.2, in the common approaches for weak pre- and postselected measurements the shift in the expectation value is calculated as follows. For a pointer observable \hat{B} , which is also the indicator, and its complementary observable \hat{C} the change of the expectation value is given by (c.f. [Kofman12, Dressel14])

$$\mathcal{D}_F(C) \approx \Gamma \operatorname{Re} [(P_A)_w] \quad (4.26)$$

$$\mathcal{D}_F(B) \approx 2\Gamma(\Delta B)^2 \operatorname{Im} [(P_A)_w], \quad (4.27)$$

where Γ is the coupling strength as defined in sec. 2.1.3 and ΔB is the uncertainty of the initial pointer

$$(\Delta B)^2 = \langle \Phi | \hat{B}^2 | \Phi \rangle - \langle \Phi | \hat{B} | \Phi \rangle^2. \quad (4.28)$$

Eq. (4.25) effectively provides the same formulas for the calculation of the shift, but derived with the new ansatz of effects of interactions [Dziewior18]. A detailed mathematical derivation can be found in the appendix B.5.

Furthermore, it can be shown that Gaussian pointer states

$$\Phi(x) = \left(\frac{1}{2\pi(\Delta x)^2} \right)^{\frac{1}{4}} e^{-\frac{(x-x_0)^2}{4(\Delta x)^2}}, \quad (4.29)$$

with x_0 as the initial x position and Δx as the uncertainty, have special properties. On the one hand eq. (4.23) and (4.25) can be written as

$$\mathcal{D}(x) = 2\epsilon \operatorname{Re} \left[\langle \Phi | \hat{x} | \Phi^\perp \rangle \right] \quad (4.30)$$

$$\mathcal{D}_F(x) = 2\epsilon \operatorname{Re} \left[\langle \Phi | \hat{x} | \Phi^\perp \rangle (P_A)_w \right]. \quad (4.31)$$

without having to consider additional terms of $\mathcal{O}(\epsilon^2)$. On the other hand, since the matrix element $\langle \Phi | \hat{\mathbf{x}} | \Phi^\perp \rangle$ is real, eq. (4.31) can be rewritten as

$$\mathcal{D}_F(x) = \mathcal{D}(x) \operatorname{Re} [(P_A)_w]. \quad (4.32)$$

Comparing this equation to formula (4.26) shows that $\mathcal{D}(x) = \Gamma$. This is one of the central results of this work and can be generalized [Dziewior18] to show that in fact any shift of a pointer expectation value for the single path of the form $\mathcal{D}(x)$ becomes modified according to the real part of the weak value for the pre- and postselected case $\mathcal{D}_F(x)$. For the Gaussian states the usual approximate equations (4.26) and (4.27) become exact expressions

$$\mathcal{D}_F(x) = \delta x \operatorname{Re} [(P_A)_w], \quad (4.33)$$

$$\mathcal{D}_F(p) = 2\delta x (\Delta p)^2 \operatorname{Im} [(P_A)_w] \quad (4.34)$$

with p as the conjugate momentum to x and $\Gamma = \delta x$. The Gaussian state eq. (4.29) is again a Gaussian in the momentum representation. Thus, by taking $\hat{\mathbf{x}}$ as the indicator, analogous expressions can be found for the momentum

$$\mathcal{D}_F(p) = \delta p \operatorname{Re} [(P_A)_w], \quad (4.35)$$

$$\mathcal{D}_F(x) = -2\delta p (\Delta x)^2 \operatorname{Im} [(P_A)_w]. \quad (4.36)$$

A further investigation of the Gaussian pointer provides the formulas for a combination of both shifts δx and δp for general complex weak values

$$\mathcal{D}_F(x) = \delta x \operatorname{Re} [(P_A)_w] - 2\delta p (\Delta x)^2 \operatorname{Im} [(P_A)_w], \quad (4.37)$$

$$\mathcal{D}_F(p) = \delta p \operatorname{Re} [(P_A)_w] + \frac{\delta x}{2(\Delta x)^2} \operatorname{Im} [(P_A)_w], \quad (4.38)$$

where $\Delta p = \frac{1}{2\Delta x}$ because Gaussian wave packets satisfy the minimum uncertainty relation $\Delta x \Delta p = 1/2$. This expression is explicitly derived in chapter 5.

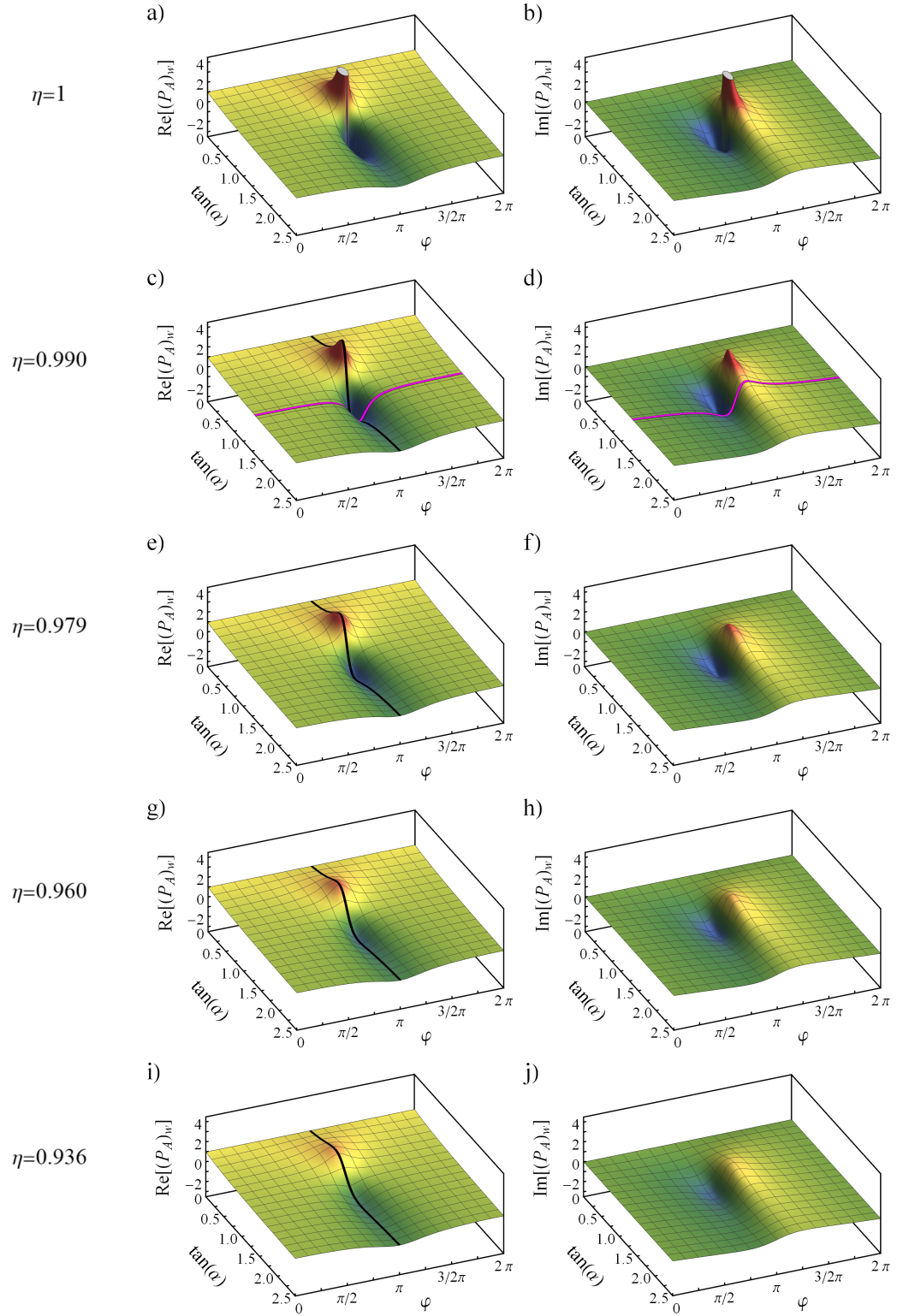


Figure 4.2: **Parameter dependence of modified weak value:** Real (left column) and imaginary (right column) part of the modified weak value is presented for $\eta = 1, 0.990, 0.979, 0.960,$ and 0.936 , dependent on the phase φ and the amplitude ratio $\tan \alpha$. The black lines correspond to the test of the parameter dependence for several η and the violet lines correspond to the test of the universality (see sec. 4.3). Adapted from [Dziewior18].

4.3 Experimental demonstration

In this section the theoretical results of the previous section 4.2, namely the universality property and the parameter dependence of the modified weak value, are demonstrated experimentally. For that purpose an optical MZI, as already presented in chapter 3 is used. Notice that figure 4.3 is slightly modified with respect to the interferometer presented in chapter 3 to focus on the important parts for the demonstration, especially how the various interactions with external systems are introduced. As done in most weak measurement experiments different degrees of freedom (DOFs) of the photon itself are regarded as the external systems, while the path degree of freedom is considered for encoding the principal pre- and postselected system of interest. There are several proposals to use distinct particles as external systems [Feizpour11, Simon11, Fu15, Ben-Israel17, Hallaji17], however hardly to be implemented with the current state of the art.

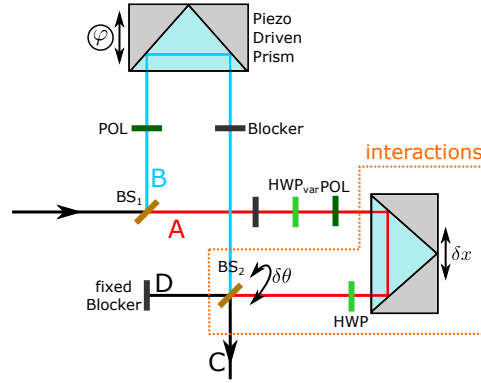


Figure 4.3: **Interferometer setup for demonstrating the universality and the parameter dependence of the modified weak value.** The figure shows basically the interferometer of fig. 3.1, but only with the necessary DOF for the introduced interactions. These are a shift δx , realized by moving the prism via the stepper motor, a momentum change $\delta\theta_y$, realized by tilting BS_2 , and a polarization shift $\delta\sigma_x$, realized by rotating the HWP.

4.3.1 Introducing the various interactions

To observe the universality three different interactions are applied, as illustrated in the orange box of fig. 4.3. These act on the spatial DOF x and y and on the polarizational DOF σ . The interactions are in good approximation independent of each other, thus the ansatz of eq. (4.19) and (4.18) is

applicable. The composite state in each arm is

$$|A\rangle|\Phi'\rangle = |A\rangle|\Phi'_x\rangle|\Phi'_y\rangle|\Phi'_\sigma\rangle|\Phi'_O\rangle \quad (4.39)$$

$$|B\rangle|\Phi\rangle = |B\rangle|\Phi_x\rangle|\Phi_y\rangle|\Phi_\sigma\rangle|\Phi_O\rangle, \quad (4.40)$$

with imperfections modeled as additional interaction acting on $|\Phi_O\rangle$.

In the given setup the photons are emitted by a laser source and thus the beams are characteristic Gaussian beams. Along the propagation direction z the transversal beam profile, and thus the initial spatial pointer state, can be well described by a Gaussian distribution. The interaction with the spatial degree of freedom is then a shift δx on the photon in arm A relative to the photon undisturbed in arm B . Hence, the final pointer state in arm A , $|\Phi'_x\rangle$, is again a Gaussian, shifted to the initial Gaussian by δx . The corresponding spatial distributions are

$$\Phi_x(x) = e^{-\frac{x^2}{w_0^2}} \quad (4.41)$$

$$\Phi'_x(x) = e^{-\frac{(x-\delta x)^2}{w_0^2}}, \quad (4.42)$$

where w_0 denotes the waist of the beam, which is given by the characteristic Rayleighrange according to $w_0^2 = z_R \lambda / \pi$ with λ as the wavelength of the photons. Note that the normalization factor is omitted (c.f. (4.29)) to focus on the effect of the interaction on the pointer state. For the realization of this spatial shift in x , the prism in arm A is moved by a stepper motor, as depicted in fig. 4.3.

In y the interaction is introduced as a momentum change δp_y . Also for this spatial DOF the initial and final pointer states $|\Phi_y\rangle$ and $|\Phi'_y\rangle$, are Gaussians, now in the momentum representation. The final state is shifted relatively to the initial state according to

$$\Phi_y(p_y) = e^{-\frac{p_y^2}{w_0^2}} \quad (4.43)$$

$$\Phi'_y(p_y) = e^{-\frac{(p_y - \delta p_y)^2}{w_0^2}}. \quad (4.44)$$

The change of the expectation value by δp_y can be directly measured with the given setup. In the paraxial approximation it has even a linear relation to the deflection angle of the beam in y direction $\delta \theta_y$ as

$$\delta p_y = \frac{2\pi}{\lambda} \delta \theta_y. \quad (4.45)$$

Hence a measurement of the change of the expectation value of θ_y corresponds to a measurement of the shift in the expectation value of p_y . This interaction can be approximately realized by tilting BS₂ as depicted in fig.

4.3. For more details see sec. 3.2.2.

The third interaction acts on the polarization state of the photon $|\Phi_\sigma\rangle$, which is initially horizontally polarized, i.e., $|H\rangle$. By introducing a polarization shift $\delta\sigma_x$ the initial and final states are given by

$$|\Phi_\sigma\rangle = |H\rangle \quad (4.46)$$

$$|\Phi'_\sigma\rangle = \cos \frac{\delta\sigma_x}{2} |H\rangle + \sin \frac{\delta\sigma_x}{2} |V\rangle. \quad (4.47)$$

The polarization shift is set by means of the HWP in arm A , while keeping the polarization in arm B fixed to $|H\rangle$.

Notice that the introduced interactions have an effect on various physical properties of the photon, thus on various external systems.

4.3.2 Observation of the universality of the weak value

One way to demonstrate the universality of the weak value of the projection operator is to perform a tomography of the final pointer states for the pre- and postselected case to confirm eq. (4.21) for quantum states. However, the property of universal modification can just as easily be seen from the change of the expectation values. In table 4.1 the introduced interactions are summarized in terms of the corresponding indicators $\hat{\mathbf{B}}$ and their complementary observable $\hat{\mathbf{C}}$. The changes of the expectation values, which can be observed for the postselected external systems \mathcal{D}_F compared to the change observed after passing only one path \mathcal{D} , have been derived in [Dziewior18].

Table 4.1: Summary of interactions applied on the PPS with corresponding indicators $\hat{\mathbf{B}}$, their complementary observables $\hat{\mathbf{C}}$ and the calculated change according to eq. (4.26) and (4.27), which were derived in [Dziewior18]. z_R denotes the Rayleigh range with $z_R = \pi w_0^2/\lambda$.

DOF	$\hat{\mathbf{C}}$	$\hat{\mathbf{B}}$	$\mathcal{D}_F(C)$	$\mathcal{D}_F(B)$
x	$\hat{\mathbf{x}}$	$\hat{\theta}_{\mathbf{x}}$	$\mathcal{D}(x) \text{Re} [(P_A)_w]$	$\mathcal{D}(x)/z_R \text{Im} [(P_A)_w]$
y	$\hat{\theta}_{\mathbf{y}}$	$\hat{\mathbf{y}}$	$\mathcal{D}(\theta_y) \text{Re} [(P_A)_w]$	$-z_R \mathcal{D}(\theta_y) \text{Im} [(P_A)_w]$
σ	$\hat{\sigma}_{\mathbf{x}}$	$\hat{\sigma}_{\mathbf{y}}$	$\mathcal{D}(\hat{\sigma}_{\mathbf{x}}) \text{Re} [(P_A)_w]$	$-\mathcal{D}(\hat{\sigma}_{\mathbf{x}}) \text{Im} [(P_A)_w]$

For demonstrating the universality property a three-stage-measurement has been performed:

- 1) Measurement of arm B alone (by blocking arm A)
- 2) Measurement of arm A alone (by blocking arm B)
- 3) Measurement of the interference signal.

The first two stages together provide important information for comparing the theoretical predictions of table 4.1 to the experimental results presented

in fig. 4.5. The measurement of arm B alone is taken as reference corresponding to no interaction, which is marked as the dashed blue zero lines in fig. 4.5. By considering the results of step 1, the effects of the interactions on arm A alone $\mathcal{D}(x)$, $\mathcal{D}(\theta_y)$, and $\mathcal{D}(\sigma_x)$ can be determined in step 2, which are depicted as dashed red lines in the upper row of fig. 4.5. Analogously, in the lower row the red line shows the change in the expectation value of the various indicator observables, which have been kept as close as possible to zero in the experiment. This is necessary to observe the behavior, which is predicted in table 4.1. Notice that the measurement results of step 1 and 2 are phase independent, so only the mean values of the shifts are depicted in fig. 4.5.

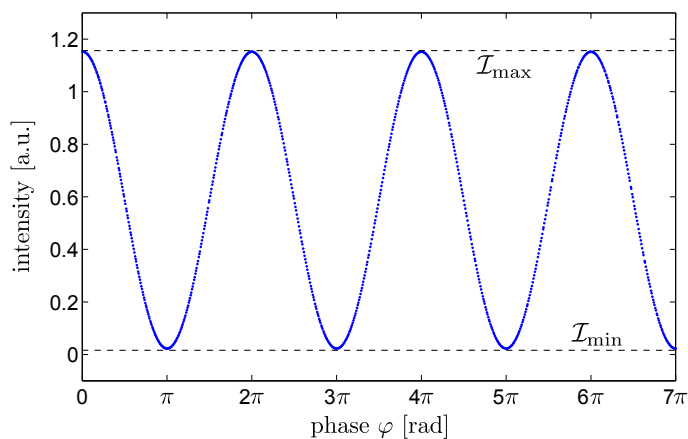


Figure 4.4: **Interference signal dependent on phase:** After the phase correction to every measured data point at the same time a certain phase φ is assigned, here displayed for the example of the interference signal. With the maximal and minimal intensity of the interference (\mathcal{I}_{\max} and \mathcal{I}_{\min}) the visibility \mathcal{V} can be determined, which is used to calculate the parameter η of the weak value.

With the first two measurement stages the parameter $\tan \alpha$ for the phase dependent weak value can be evaluated to 1.3323 ± 0.0002 according to eq. (4.10). The other parameters needed to evaluate $(P_A)_w$ (eq. (4.14)), the phase φ and the overlap η , are obtained from the last measurement step. A sinusoidal fit of the intensity of the interference signal \mathcal{I} , which is proportional to the recorded output power, yields the corresponding phase φ . A detailed description of this method is given in the appendix A.2.1 and an exemplary result is shown in fig. 4.4. With the intensity of the interference signal the visibility \mathcal{V} and subsequently the overlap η can be determined,

according to (c.f. [Dziewior18])

$$\mathcal{V} \equiv \frac{\mathcal{I}_{\max} - \mathcal{I}_{\min}}{\mathcal{I}_{\max} + \mathcal{I}_{\min}} = \eta \frac{2 \tan \alpha}{1 + \tan^2 \alpha}, \quad (4.48)$$

with \mathcal{I}_{\max} as the maximal and \mathcal{I}_{\min} as the minimal intensity of the interference signal (as shown in fig. 4.4). In the performed experiment $\mathcal{V} = (95.09 \pm 0.02)\%$ and $\eta = 0.9904 \pm 0.0003$. Taking these parameters amplification factors from -3 up to 4 can be achieved, as shown in fig. 4.2 c) and d).

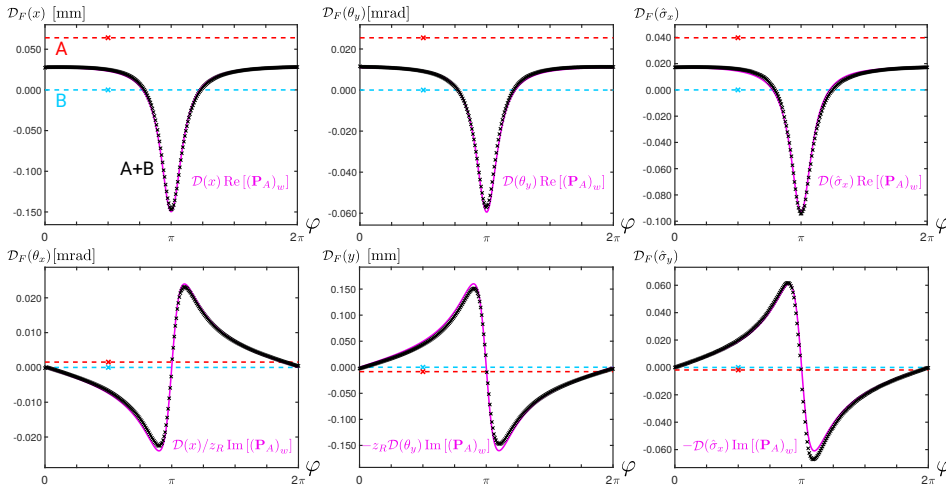


Figure 4.5: Observation of universality: The upper row shows the introduced displacements (δx , $\delta \theta_y$, $\delta \sigma_x$) in arm A for the single arm measurements as phase independent dashed red lines and for the PPS measurement as phase dependent crosses with the theoretical prediction according to table 4.1 as solid violet lines. The measurement of arm B is taken as reference and corresponds to the blue zero lines in all plots. Analogous, the lower row shows the measured displacements for the complementary observables. The similarity in the behavior for all three DOF, which is modified by the weak value, clearly shows the universality property. Adapted from [Dziewior18].

In fig. 4.5 the theoretical predictions of table 4.1 as well as the measured interference signal for the three different couplings are presented. The first row shows the shift in the expectation values $\hat{\mathbf{C}}$ for the different degrees of freedom and the second row shows the changes of the indicator observable $\hat{\mathbf{B}}$. In each plot the relative shift of the single arms is indicated with \mathcal{D} , and of the relative shift of the interference signal, i.e. the signal after postselection, is indicated with \mathcal{D}_F . Note that because the position sensing detectors are not perfectly placed in the waist or in the far field of the beam, the data for the spatial interactions were postprocessed according to section

3.2.1 to obtain \mathcal{D} and \mathcal{D}_F . Furthermore, the results of the interference measurement depicted in fig. 4.5 is the mean over several periods to average out fluctuations. According to table 4.1 the first row should exhibit a relation to the real part and the second row to the imaginary part of the weak value. And indeed, the measured interference signal, which is marked as black crosses, fits very well to the theoretical predictions depicted as violet lines in the corresponding plot. The small discrepancies, especially by comparison of $\mathcal{D}_F(B)$ between experimental data and theory, are mainly due to systematic errors. These results are remarkable in the sense that the effects of different physical interactions are all modified the same way. This shows clearly the universality of $(P_A)_w$ for the interferometric PPS.

4.3.3 Parameter dependence of modified weak value

To see that the description of the modified weak value (eq. (4.14)) is valid, it is necessary to test in particular the dependence on the new introduced parameter η , which denotes the overlap (see eq. (4.2)), i.e., the coherence between the two arms. It depends on the introduced interactions, thus, changing them also changes η . As already mentioned, the different interactions are approximately independent of each other, hence eq. (4.19) holds and thus also η can be expressed in product form

$$\eta = \eta_x \cdot \eta_y \cdot \eta_\sigma \cdot \eta_O, \quad (4.49)$$

which are defined according to (4.2). In this formula η_O denotes the modified overlap due to imperfections of optical devices and

$$\eta_x = \exp\left(-\frac{\delta x^2}{2w_0^2}\right) \cdot \exp\left(-\frac{\delta\theta_x^2 z_R^2}{2w_0^2}\right) \quad (4.50)$$

$$\eta_y = \exp\left(-\frac{\delta y^2}{2w_0^2}\right) \cdot \exp\left(-\frac{\delta\theta_y^2 z_R^2}{2w_0^2}\right) \quad (4.51)$$

$$\eta_\sigma = \cos\left(\frac{\arcsin(\delta\sigma_x)}{2}\right) \quad (4.52)$$

denote the overlap in the various degrees of freedom in which some interaction was introduced, where z_R is the Rayleigh range with $z_R = \pi w_0^2/\lambda$. As it can be seen from eq. (4.49) the overlap can either be changed by the spatial DOFs or by the polarization DOF. Because of the experimental realization of the setup (fig. 3.1) the simplest and most reproducible way to modify η is by rotating the HWP, thus changing η_σ .

Furthermore, since in the previous section the weak value was only evaluated for fixed $\tan\alpha$, now also the dependence on this parameter should be investigated. For that purpose different intensity ratios are set, as described in sec. 3.1.3 but with an additional neutral density filter, placed

in arm B just before the second BS. With this configuration it is possible to set $\tan \alpha \gtrsim 0.7$, but indeed for our purpose it is enough to measure up to $\tan \alpha \lesssim 2.5$, since the interesting dependence can be observed close to $\tan \alpha = 1$, i.e., equal transmission through path A and B .

The measurement procedure is the same as described in sec. 4.3.2, but now evaluating only the data at $\varphi = \pi$. This value for φ is chosen because the imaginary part of the weak value vanishes for this parameter set and thus the amplification happens solely due to the real part of the weak value, which is furthermore maximal for $\varphi = \pi$ as it can be seen in the surface plots 4.2.

Fig. 4.6 shows the measured maximal amplification for $\eta = 0.990, 0.979, 0.960$, and 0.936 as dots with error bars, and the theoretical curves as solid lines for the measured η with an additional curve for $\eta = 1$. The error is the sum of a systematic error and a statistical error. The systematic error is due to the behavior of the PSDs themselves which increases for $\tan \alpha$ close to 1 (see appendix A.2.2). The statistical error is constituted by the statistical error in the reading of the position and by the statistical error due to fluctuations. The theoretical behavior of the weak value for the presented overlaps was already described in sec. 4.2.1. Fig. 4.6 shows that the experimental data fit very well to the theory, which demonstrates the validity of the weak value given by eq. (4.14).

Note, high weak value amplifications can be obtained only for (almost) perfect overlap. Already for $\eta = 0.99$ (corresponding to a visibility $\mathcal{V} \sim 95\%$) the maximum value reduces to ~ 4 .

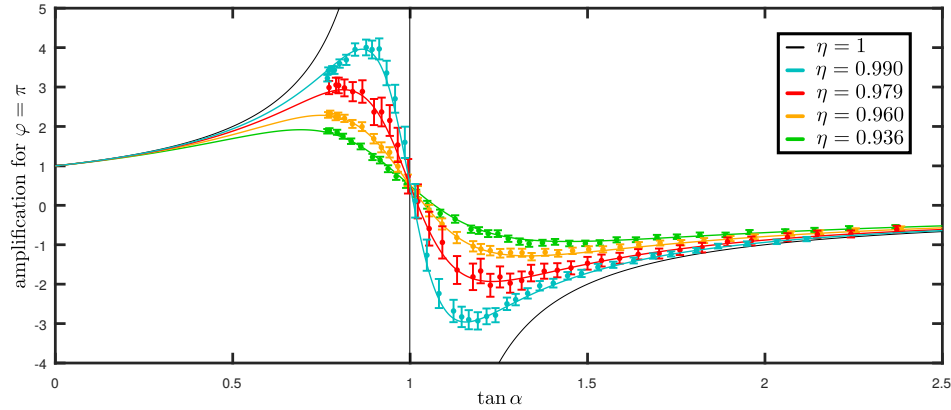


Figure 4.6: **Modification of weak value due to loss of coherence:** The figure shows the amplification factors according to eq. (4.14) for fixed $\varphi = \pi$ tested for different overlaps η by varying the intensity ratio $0.7 \lesssim \tan \alpha \lesssim 2.5$. The dots show the measured data and with solid lines as corresponding theoretical curves. Adapted from [Dziewior18].

4.4 Conclusion

In this chapter the question, whether the weak value concept is valid for multiple interactions, has been investigated in the framework of a Mach-Zehnder interferometer. For this purpose an extended description of the effects of interactions on external systems has been introduced, namely the appearance of some orthogonal component to the initial external system state. Subsequently, this ansatz was applied in the interferometer, with only one arm containing multiple interactions.

Using this approach it has been possible to consider the loss of coherence of the system state due to the various interactions of finite strength and imperfections of optical components. This insight yielded a modified formula for the weak value of the projection operator onto the arm, in which the interactions take place. The parameter dependence of the modified weak value on the overlap η , the amplitude ratio $\tan \alpha$ and the phase between the two arms of the MZI φ has been validated in good agreement with experimental data.

Furthermore, the universality of the weak value in the presented interferometric PPS has been shown theoretically and experimentally. For the experimental demonstration various interactions concerning either a shift δx , a momentum change $\delta \theta_y$, or a polarization shift $\delta \sigma_x$ in the different degrees of freedom of the photon have been introduced. All of them exhibited the characteristic-universal-modification in the shifts of the expectation values of the corresponding observables.

In summary, these results show that the introduced modified weak value in the Mach-Zehnder interferometer is not only a valid concept but, furthermore and more importantly, it is a universal modification factor for the effects of any and every interaction of a pre- and postselected system.

Chapter 5

Alignment of interferometers using weak values

5.1 Introduction

In the previous chapter the universality of the weak value of the projection operator was derived. In this chapter it is shown how this property can be used for the alignment of an interferometer.

Interferometers itself are an important tool for a variety of experiments, e.g., for the disprove of the theory of luminiferous aether [Michelson31], for the development of ultrahigh-resolution full-field optical coherence tomography [Duck89], for the detection of earth's rotation [Anderson94], and for the most popular recent discovery of gravitational waves [Abbott16]. However, before an interferometer can be utilized, the two arms have to be precisely aligned. The alignment process itself is often a very time consuming procedure. The universality of the weak value inspired an alignment technique presented in this chapter, which indeed was already utilized in [Danan13] and further developed in [Farfurnik13, Benshalom17].

To derive the formulas for the alignment technique based on the weak value concept, first we want to investigate the employed external systems, i.e., Gaussian pointers, in the case of strong interactions. The next step is to consider how the misalignment of an interferometer can be described by interactions. With these results and the universality property of the weak value of the projection operator (see chapter 4) finally a formula for the centroid of the interference signal is provided, on which the alignment procedure is based on. This procedure is presented and demonstrated experimentally for two different positions of the spatial detector and for two different coupling strengths.

5.2 Theoretical considerations

First, we want to derive the formula on which the alignment procedure is based on. For this purpose, we have a closer look on the external systems. As already mentioned in sec. 4.3.1 the spatial external systems can be well described by Gaussian distributions, because it is the characteristic transversal beam profile for a Gaussian beam. Thus, the pointer state in one spatial degree of freedom can be described as Gaussian wave packet, which is initially given by eq. (4.29). The uncertainty Δx for a Gaussian beam is determined by

$$4(\Delta x)^2 = w_0^2 = z_R \frac{\lambda}{\pi}, \quad (5.1)$$

with the Rayleigh range z_R and the minimal extension of the waist w_0 . In our case $z_R = 4.1$ m, as already mentioned in sec. 3.1.1.

5.2.1 Gaussian pointers considered for strong interactions

It can be proven that in the special case of Gaussian pointers equation (4.26) and (4.27) become exact, and thus hold even in the strong interaction regime. The complete proof is reprinted with permission in the appendix B.6, whereas in this section it is only sketched.

For the proof arbitrary pre- and postselected systems are considered, whose states can be represented by density matrices. The initial state of system and pointer is assumed to be unentangled, hence can be expressed by a product state analogous to eq. (2.8). The second assumption is that the interaction between the pre- and postselected system (PPS) and the pointer can be described with the von Neumann model, thus with a unitary evolution. As already described in section 2.1.3, this can be parametrized as in eq. (2.12), with operator $\hat{\mathbf{A}}$ acting only on the PPS and $\hat{\mathbf{B}}$ acting only on the pointer. Moreover, we require for $\hat{\mathbf{A}}$ that it commutes with all other evolutions of the system and the environment, which are in a similar form as in eq. (2.12). With this requirement fulfilled the ordering of the respective evolutions becomes time-independent. As already explained in section 4.2.1, this allows us to choose the moment to evaluate the weak value just before postselection in the Mach-Zehnder interferometer.

The first step in the proof is the calculation of the expectation value of the postselected pointer state according to eq. (2.17). For this purpose the postselected pointer state can be determined by taking the partial trace of the final composite state over the system. Next, we calculate the weak value of the projection operator in a MZI. The comparison of these results yields the following conditions with respect to the initial pointer state expressed

by a density matrix ϕ_0

$$\text{Re} \left[\text{Tr} \left(\phi_0 \hat{\mathbf{B}}^k \hat{\mathbf{C}} \right) \right] = \text{Tr} \left(\phi_0 \hat{\mathbf{C}} \right) \text{Tr} \left(\phi_0 \hat{\mathbf{B}}^k \right), \quad (5.2)$$

$$\text{Im} \left[\text{Tr} \left(\phi_0 \hat{\mathbf{B}}^k \hat{\mathbf{C}} \right) \right] = -\frac{k}{2} \text{Tr} \left(\phi_0 \hat{\mathbf{B}}^{k-1} \right), \quad (5.3)$$

$$\text{Tr} \left(\phi_0 \hat{\mathbf{B}}^{k+1} \right) = \text{Tr} \left(\phi_0 \hat{\mathbf{B}} \right) \text{Tr} \left(\phi_0 \hat{\mathbf{B}}^k \right) + 2(\Delta B)^2 \text{Tr} \left(\phi_0 \hat{\mathbf{B}}^{k-1} \right), \quad (5.4)$$

with k as the exponential number, and $\hat{\mathbf{B}}$ and $\hat{\mathbf{C}}$ fulfilling the commutator relation $[\hat{\mathbf{C}}, \hat{\mathbf{B}}] = i$.

The second step is to check the conditions (5.2) - (5.4) for Gaussian pointers. For the investigated scenario in this chapter, we consider the Gaussian state $|\Phi_j\rangle$ in spatial representation, thus $\hat{\mathbf{C}} = \hat{\mathbf{x}}$ and $\hat{\mathbf{B}} = \hat{\mathbf{p}}$ and vice versa for the case of a momentum shift. Considering the initial state $|\Phi_j\rangle$ as pure state, the first two conditions can be checked by calculating the twofold expectation value $\langle \Phi_j | \hat{\mathbf{p}}^k \hat{\mathbf{x}} | \Phi_j \rangle$. By using eq. (2.22), for a Gaussian state the twofold expectation value can be rewritten by

$$\langle \hat{\mathbf{p}}^k \hat{\mathbf{x}} \rangle = -\frac{i}{2(\Delta p)^2} \left(\langle \hat{\mathbf{p}}^{k+1} \rangle - \langle \hat{\mathbf{p}} \rangle \langle \hat{\mathbf{p}}^k \rangle \right) + \langle \hat{\mathbf{x}} \rangle \langle \hat{\mathbf{p}}^k \rangle, \quad (5.5)$$

which is derived in the appendix (B.7). From this result the validity of the first condition (5.2) is obvious. By inserting eq. (5.5) into the second condition (5.3) it modifies to the third condition (5.4). The validity of the third condition for the Gaussian state can be proven by calculating the expectation value $\langle \hat{\mathbf{p}}^{k+1} \rangle$ using the recursive relation of momentum expectation values for Gaussian states, which for $\langle \hat{\mathbf{p}} \rangle = 0$ is

$$\langle \hat{\mathbf{p}}^{k+1} \rangle = k(\Delta p)^2 \langle \hat{\mathbf{p}}^{k-1} \rangle. \quad (5.6)$$

By these calculations it has been proven, that Gaussian states satisfy the required conditions and therefore the shift of the expectation value is related linearly to the weak value of the projection operator even for strong interactions.

5.2.2 Misalignment as interaction

In the previous chapter the universality property of the weak value of the projection operator was already considered for a position shift in x and a momentum kick in y . A combination of both types of effects in every spatial degree of freedom exactly describes the scenario of a misaligned interferometric setup. Thus, the misalignment can be described by a weighted sum of the interactions generated by $\hat{\mathbf{x}}$ and $\hat{\mathbf{p}}$. By considering arm B again as reference, the interaction can be parametrized as occurring only in arm A . Hence, the shifted pointer state can be described by

$$|\Phi'\rangle = e^{-i(\Gamma_{p_x} \hat{\mathbf{x}} + \Gamma_x \hat{\mathbf{p}})} |\Phi\rangle, \quad (5.7)$$

where Γ_x and Γ_{p_x} denote the corresponding interaction strengths respectively. By considering the spatial Gaussian function of eq. (4.29) for $x_0 = 0$ this becomes

$$\Phi'(x) = \langle x | \Phi' \rangle = \langle x | e^{-i(\Gamma_{p_x} \hat{x} + \Gamma_x \hat{p})} | \Phi \rangle \quad (5.8)$$

$$= \left(\frac{1}{2\pi(\Delta x)^2} \right)^{\frac{1}{4}} e^{-\frac{(x-\Gamma_x)^2}{4(\Delta x)^2}} e^{-i\Gamma_{p_x} x}. \quad (5.9)$$

The shift in the expectation value in only one arm can be determined to

$$\mathcal{D}(x) = \langle \Phi' | \hat{x} | \Phi' \rangle = \Gamma_x = \delta x, \quad (5.10)$$

$$\mathcal{D}(p) = \langle \Phi' | \hat{p} | \Phi' \rangle = -\Gamma_{p_x} = -\delta p_x. \quad (5.11)$$

Next, we want to calculate the shift after the postselection. The pointer state after postselection in output port C , i.e., $|\Phi_F\rangle$ is a superposition of the states $|\Phi'\rangle$ and $|\Phi\rangle$ from arms A and B respectively. It can be written as

$$|\Phi_F\rangle = \mathcal{N} (|\Phi'\rangle + \tan \alpha e^{i\varphi} |\Phi\rangle) \quad (5.12)$$

with $\tan \alpha$ quantifying the relative weight, φ the relative phase and

$$\mathcal{N}^{-2} = 1 + \tan^2 \alpha + 2 \tan \alpha \eta \cos \varphi \quad (5.13)$$

as the normalization factor. The expectation value of an operator \hat{O} is

$$\mathcal{D}_F(O) = \langle \Phi_F | \hat{O} | \Phi_F \rangle \quad (5.14)$$

$$= \mathcal{N}^2 \left[\langle \Phi' | \hat{O} | \Phi' \rangle + \tan^2 \alpha \langle \Phi | \hat{O} | \Phi \rangle + 2 \tan \alpha \operatorname{Re} \left[e^{i\varphi} \langle \Phi' | \hat{O} | \Phi \rangle \right] \right]. \quad (5.15)$$

The matrix elements of the formula (5.15) can be evaluated by using the formulas of the initial (4.29) and shifted (5.9) Gaussian state

$$\langle \Phi' | \hat{x} | \Phi \rangle = \frac{\eta}{2} (\delta x + 2i(\Delta x)^2 \delta p_x), \quad (5.16)$$

$$\langle \Phi' | \hat{p}_x | \Phi \rangle = \frac{\eta}{2} (-\delta p_x + 2i(\Delta p_x)^2 \delta x). \quad (5.17)$$

Inserting these results into eq. (5.9) yields

$$\begin{aligned} \mathcal{D}_F(x) &= \mathcal{N}^2 (\delta x (1 + \tan \alpha \eta \cos \varphi) \\ &\quad - 2\delta p_x (\Delta x)^2 \tan \alpha \sin \varphi), \end{aligned} \quad (5.18)$$

$$\begin{aligned} \mathcal{D}_F(p_x) &= \mathcal{N}^2 (-\delta p_x (1 + \tan \alpha \eta \cos \varphi) \\ &\quad - 2\delta x (\Delta p_x)^2 \tan \alpha \sin \varphi). \end{aligned} \quad (5.19)$$

By using the modified weak value (4.14) the eq. (5.15) can be rewritten and we obtain the already presented formulas (4.37) and (4.38). In this proof only a single pointer coupling to the pre- and postselected system has been considered. However, by including all other degrees of freedom in the state $|\Phi\rangle$ the proof immediately generalizes to the case of multiple pointers.

5.2.3 Derivation of the fit function

For the alignment procedure the position of the centroid of the interference pattern has to be fitted. The fit function can be derived by considering at first the position of the beam at the detector. With the paraxial approximation it can be expressed by

$$r_x \approx \mathcal{D}_F(x) + z \frac{\mathcal{D}_F(p)}{|\vec{p}|}, \quad (5.20)$$

where \mathcal{D}_F denotes the expectation value after postselection and z denotes the position of the detector along the propagation direction of the beam with respect to the position of the waist z_0 (which we defined to be the zero position). Remember that we set $\hbar = 1$, thus $|\vec{p}|$ can be calculated by $|\vec{p}| = 2\pi/\lambda$ with λ as the wavelength of the photons. In the previous section we derived the shifts $\mathcal{D}_F(x)$ and $\mathcal{D}_F(p)$ in the expectation value for a PPS in an interferometer (and obtained eq. (4.37) and (4.38)). Inserting them into eq. (5.20) yields

$$\begin{aligned} r_x \approx & \delta x \operatorname{Re} [(P_A)_w] - 2\delta p_x (\Delta x)^2 \operatorname{Im} [(P_A)_w] \\ & + \frac{z}{|\vec{p}|} (\delta p_x \operatorname{Re} [(P_A)_w] + 2\delta x (\Delta p_x)^2 \operatorname{Im} [(P_A)_w]). \end{aligned} \quad (5.21)$$

By using the uncertainty relation of a Gaussian wave packet (5.1) and the paraxial approximation for the momentum eq. (4.45) the final fit formula can be obtained

$$\begin{aligned} r_x = & \delta x \left(\operatorname{Re} [(P_A)_w] + \frac{z}{z_R} \operatorname{Im} [(P_A)_w] \right) \\ & + z_R \delta \theta_x \left(\frac{z}{z_R} \operatorname{Re} [(P_A)_w] - \operatorname{Im} [(P_A)_w] \right). \end{aligned} \quad (5.22)$$

The complete calculation is shown in the appendix B.8. Analogously to eq. (5.22) the misalignment in y can be determined.

5.3 Experimental demonstration

5.3.1 Alignment procedure

The alignment technique is based on the previous theoretical insights, namely the concept to consider misalignments as an interaction causing changes on

all degrees of freedom of the beam, the special properties of Gaussian pointer even in the strong interaction regime, and the strong phase dependence of the weak value and the interference signal. These insights can be exploited by employing the following procedure:

- 1) Record (at least) a 2π phase scan of the centroid of the interference pattern by means of a position resolving detector.
- 2) Perform a least square fit of the phase dependent position separately in the different spatial degrees of freedom x and y using eq. (5.22) to obtain the misalignment parameters δx , $\delta\theta_x$, δy , and $\delta\theta_y$.
- 3) Realign according to the provided misalignment parameters.
- 4) Optional: Measure the new misalignment parameters and, if necessary, repeat step 2 and 3.

The implementation of this procedure has been done with the setup presented in chapter 3 (without considering the polarization analysis), in which also the working principle of the setup has been explained. Still, some of the experimental parts are mentioned again to emphasize their relation to the various alignment steps.

In fig. 5.1 two different runs of the alignment procedure with position sensing detectors (PSDs) located at different positions along the propagation direction are depicted. The left column corresponds to a run evaluated with PSD₁ (at $z = -0.24$ m) and is denoted by I , the right column corresponds to a different run evaluated with PSD₂ (at $z = 5.27$ m) and is denoted by II . Moreover, the two runs were taken for two different interaction strengths, as it can be seen from the effective shift shown in table 5.1 for Ia and IIa. Every row in fig. 5.1 represents another measurement step, as described in the following.

The first step is realized by means of the piezo driven prism and the PSDs. The periodical movement of the prism changes the phase φ between the two arms and thus the preselected state, resulting in a variation of the centroid (according to eq. (5.22)). Note that the phase scan has to be at least one period long that the fitting procedure works. In principle it is possible to scan over several periods to average technical fluctuations out. However, to prove the efficiency of the method for the presented runs, the centroid of the interference signal was recorded over a 2π scan on the PSD, which is depicted as in the first row of fig. 5.1 as black crosses. They can be compared to the single arm measurements, which are taken for comparison but not used for the alignment. Arm B (blue crosses) as reference measurement is located at the origin, whereas the position of arm A (red crosses) illustrates the measured misalignment without interference. The measurements of the single arms were taken during 15 seconds to analyze the single arm jittering.

Table 5.1: Obtained misalignment parameters before realigning (run Ia and IIa) and after realigning (Ib and IIb). Run I correspond to the alignment procedure with PSD₁ and run II to that with PSD₂.

run	δx [μm]	$\delta\theta_x$ [μrad]	δy [μm]	$\delta\theta_y$ [μrad]
Ia	49 ± 2	0.2 ± 0.4	7 ± 2	12.7 ± 0.4
Ib	-1 ± 2	-0.6 ± 0.4	2 ± 2	0.2 ± 0.4
IIa	74 ± 5	0.5 ± 0.8	-5 ± 5	10.8 ± 0.8
IIb	1 ± 5	1.4 ± 0.8	1 ± 5	0.9 ± 0.8

The second step consists mainly of the postprocessing of the recorded data, namely to correlate the measured data with the corresponding phase and the fitting procedure itself. The determination of the phase is done as described in the appendix A.2.1. This step of the alignment technique is depicted in the second row of fig. 5.1, in which the crosses correspond to the measured position depending on the phase and the solid lines correspond to the fit curves given by (5.22). Indeed, for improving the fitting procedure the freedom of the fit has been constrained by the additional measurements of arm *A* and *B* alone. These additional measurements provided the parameters $\tan \alpha$, and, by the evaluation of the visibility, also the overlap η (see eq. (4.48)). For run I and II the same $\tan \alpha = 0.774 \pm 0.002$ has been set. The initial overlap has been determined to 0.9938 ± 0.0003 for run Ia and to 0.9905 ± 0.0003 for run IIa from the initial visibilities $(96.14 \pm 0.02)\%$ and $(95.93 \pm 0.02)\%$. By inserting these values into formula (5.22) the least square fit yielded the misalignment parameters shown in table 5.1. Note that for the determination of the misalignment the two positions of the light from *A* and from *B* are not sufficient whereas the phase dependence of the centroid suffices to determine them only using a single PSD. This is shown in sec. 5.2.3 and demonstrated experimentally in run I and II.

The misalignment can be corrected as described in sec. 3.2.2, i.e., by means of the two tilting angles of the second beam splitter (BS₂) and by tilting and shifting the prism in arm *A*. The results of the alignment is shown in table 5.1 as Ib and IIb, the corresponding trajectories are depicted in the third row of fig. 5.1. After the realignment the visibility increased to $(96.44 \pm 0.02)\%$ for Ib and $(96.35 \pm 0.02)\%$ in IIb with the respective overlaps 0.9961 ± 0.0003 and 0.9955 ± 0.0003 .

The last step of the alignment procedure is optional and only necessary, if the beams cannot be aligned with suitable precision. For a perfect alignment the elliptical trajectory of the interference signal reduces to a point. However, the inserted zoom of the third row shows a residual ellipse, due to still imperfect alignment.

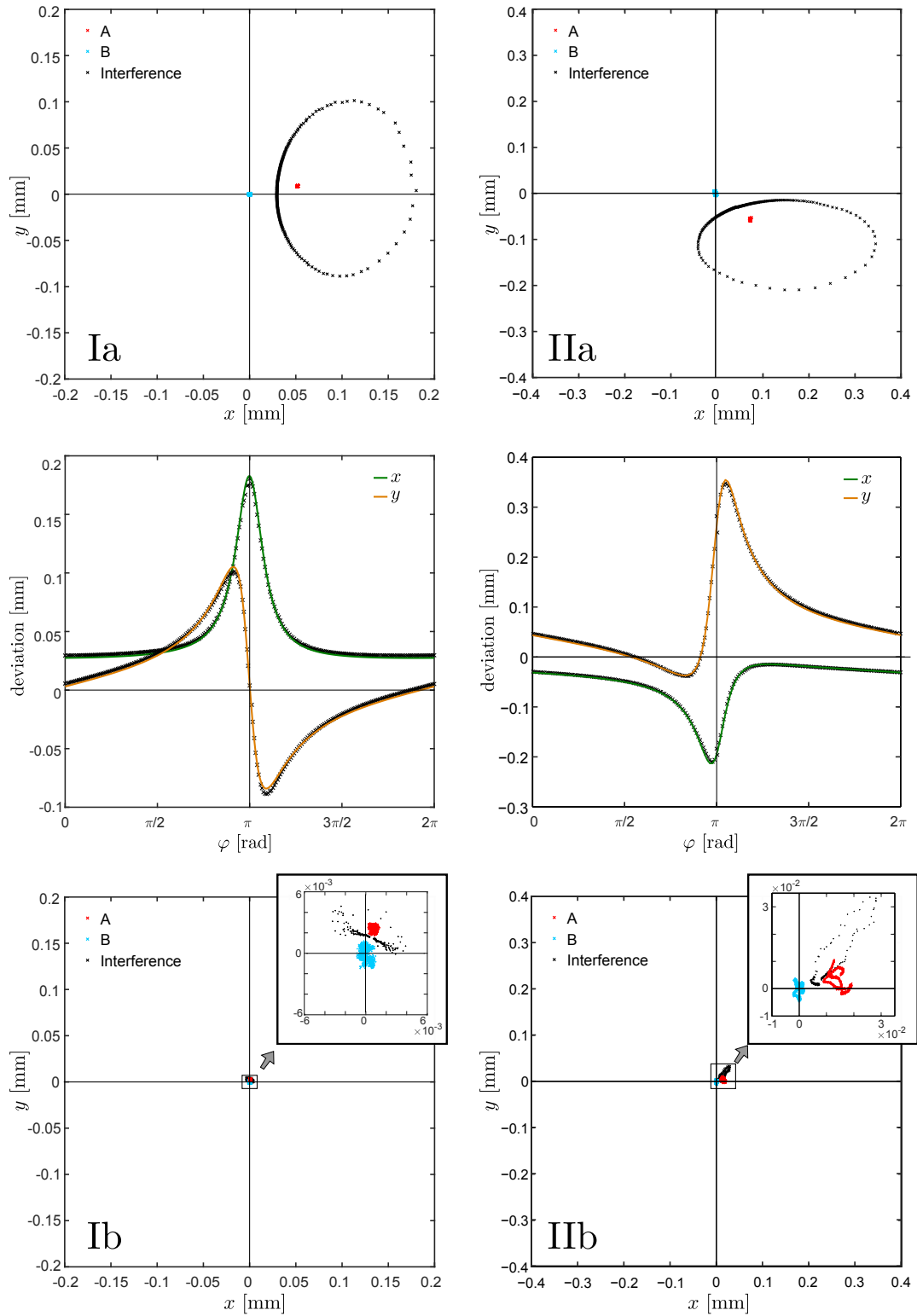


Figure 5.1: **Alignment procedure:** The different columns represent two runs for different misalignments with the PSD located at different positions. The various rows correspond to the various alignment steps, described in sec. 5.3.1. The first and the third row show the trajectories of the interference pattern before and after the alignment. The second row depicts the least square fit according to eq. (5.22), which yields the misalignment parameter. Adapted from [Dziewior18].

5.3.2 Discussion

First, we want to discuss the results of the previous section. With the presented procedure it was possible to align to the order of the fluctuations. However, the presence of a clear elliptic trajectory in the insets in Ib and IIb of fig. 5.1, suggests that the beams are not perfectly aligned. This has two reasons. The first is that the beams are indeed not perfectly aligned. In our case this is not due to false misalignment parameters but rather because the accuracy of the manual correction was limited. Especially, the setting of the desired angles (as described in section 3.2.2) is problematic. For all corrections the beam in arm B is blocked and the position of arm A has been observed with one of the PSDs. The applied angle has a direct relation to the effective position shift on a detector, which depends only on its distance to the optical component. Thus, to apply a certain angle, one has to shift the spot on the detector by a certain distance. However, this live monitoring has the disadvantage that the beam fluctuates on a time scale of seconds during the alignment process, hence the introduced shift is dependent on the fluctuation in this moment. For example, this problem could be overcome by motorizing the screws. As a consequence only the certainty of calibration and the precision of the motorized screw itself limit the accuracy of the applied shift. Furthermore, such screws could lead to a fully automatized alignment procedure, which was demonstrated in [Benshalom17]. However, also the screws cannot provide a solution for thermal fluctuations. These only can be minimized by shielding the setup.

The second reason for the comparatively large size of the residual ellipse in the insets of Ib and IIb is the increase in the weak value amplification. As eq. (4.14) shows, the weak value depends on the overlap η . The better the two beams are aligned, the higher is η . Hence, the modification values, i.e., the weak value, can reach a higher maximum. Therefore, even negligible discrepancies between both beams can cause a large effect in the interference signal.

In sec. 5.3.1 we demonstrated that the alignment procedure works within one 2π phase scan and with a single detector. These features make this technique efficient. In principle, every interferometer can implement this alignment procedure. The only requirements are the possibility to shift the phase between the two arms in a controlled way and the possibility to place a position resolving detector somewhere behind one of the output ports. Despite the efficiency and the possibility of easy implementation, it is of course difficult to provide a definite argument for the superiority of a particular experimental procedure, since a lot of practical factors have to be considered. Still it can be argued that the presented can beat other alignment procedures with respect to several key points.

The most obvious reasons are the standard arguments regarding the weak value amplification, namely that some types of technical noise can be over-

come. Since the method utilizes the interference pattern of the two beams it is sensitive only to those components of the spatial modes which are coherent. Thus, in typical cases it will optimize alignment with respect to achievable interferometric visibility. For example in the presence of asymmetric secondary reflections in one of the beams this would not be achieved by a procedure which considers only the centroids of the single beams. A further supporting argument is that the fit routine can also be used the other way round, namely to determine the parameters of the beam, for example z_R etc., for a given misalignment. These parameters are sometimes not easily accessible in an experiment with sufficient precision.

The parametrization of the scenario as a PPS with the corresponding weak value is of course not the only possible way to derive the alignment procedure. Indeed, the misalignment parameters can also be obtained by considering the problem with classical wave optics in the same manner. The universality property of the weak value inspired the presented alignment technique.

5.4 Conclusion

In this chapter an efficient alignment method for interferometric setups was presented. The investigation of the used external systems, i.e., Gaussian pointers, was an important aspect for the derivation of this technique. In particular, it has been proven that Gaussian pointers are very special in the sense that the derived approximated expressions for the shift of the expectation value in a postselected system (eq. (4.26) and (4.27)) become exact [Dziewior18]. This fact allowed us to give an exact expression for a shift of the position and the momentum and to relate it to a possible misalignment of the interferometer defining the pre- and postselected ensemble. By considering the universality property of the weak value of the projection operator, namely that the shifts generated by $\hat{\mathbf{x}}$ and $\hat{\mathbf{p}}$ are modified in the same way, a phase dependent fit function for the misalignment parameters was provided [Dziewior18]. This leads to the alignment procedure, which in principle only needs one 2π phase scan and a single position resolving detector. It was demonstrated for two different positions of the detectors and for two different coupling strengths that the interferometer could be aligned in only one run. Although the superiority of the method was not shown in this thesis, the discussed features are interesting in the light of further applications.

Chapter 6

Summary and outlook

The weak value concept describes the effects due to a weak measurement of an observable in a pre- and postselected system. In the measurement process the system of interest and the measurement system, whose quantum state is denoted by the *pointer state*, interact with each other. The aim of this thesis was to examine the modification of the pointer states in terms of the weak value, when several interactions are introduced in one arm of a Mach-Zehnder interferometer.

For the calculation of the weak value of the projection operator onto the arm in which the interactions are localized, for the first time also the coherence loss of the system of interest taken into account. The coherence loss could be caused by imperfections of optical components and interactions of finite strength, which resulted in an entanglement between the system of interest and the various pointer systems. This approach led to a modified weak value formula, which differs from the naively calculated formula by considering the overlap η of the pointer state before and after the interactions. The validity of the formula has been demonstrated experimentally for several fixed η at the fixed phase of maximum amplification by varying the intensity ratio of the two arms. The measured data were in good agreement with the theoretical predictions and therefore confirmed the modified weak value formula.

For the evaluation of the effect on the various pointer systems caused by different, sequential interactions a new description was introduced. An additional component that is orthogonal with respect to the initial pointer state appeared due to the interaction, which manifested itself as a shift in the expectation value of an observable. Using this concept led to the insight that any effect of the interactions is modified in the same universal manner, i.e., by the weak value. This is the most important result of this thesis (see also [Dziewior18]). The universality property was not only shown theoretically but also demonstrated experimentally by applying three different couplings causing shifts in position, momentum, and polarization to the photon in the

interferometer. Again, the experimental data were in good accordance with our theoretical predictions and thus confirmed the universality property of the weak value.

Furthermore, in this thesis a practical application was inspired by the universal modification due to the weak value, namely the alignment of an interferometer. In this context it was proven that in the special case of Gaussian states of the pointer the formulas for the shift in the expectation value caused by an interaction with a pre- and postselected system become exact, which is not the case in general. By considering the misalignment of the interferometer as an interaction causing displacement and directional change of the beam a fit formula for the phase dependent centroid position of the interference signal has been derived. Based on this fit an alignment procedure for interferometers has been found, which is efficient and easy to implement. The procedure was demonstrated for different coupling strengths and for different locations of the position resolving detector.

These results represent a new insight in the properties of weak values. A further step could be to prove the universality of the weak value not only for the projection operator but for any operator. Furthermore, the description of the effect of interactions on the pointer, namely taking into account the orthogonal component with respect to the initial pointer state, yields arguments for the discussions about the *trace of a photon* (c.f. [Dziewior18]). Aside from that, the controversially discussed concept of the weak value yields a further practical application, namely the alignment of an interferometer. Some of the advantages of the presented alignment technique were discussed, but it is up to future work to investigate under which circumstances it can be superior to other methods.

Appendices

Appendix A

Setup

A.1 Optical components

The employed optical components are explained here in more detail. For a more complete description, we refer to [Hecht87, Saleh91].

A.1.1 Polarizers

A linear polarizer is an optical device to control the polarization of the passing light. Only the part of the electromagnetic field, which is parallel to the transmission axis, is transmitted. The orthogonal component is blocked, which can be realized in different ways. In the setup of this thesis the blockade is done with polarizers consisting of dichroic materials, which selectively absorb the light depending on the direction incident electric field [Saleh91].

A.1.2 Waveplates

Waveplates or retarder plates are optical transparent devices which can manipulate the polarization of light traveling through it. Due to their birefringence the light has different propagation velocities in the ordinary (polarized perpendicular to optical axis) and extraordinary (polarized parallel to optical axis of the components) axes. The phase difference of beams traveling through the different axes is given by [Saleh91]

$$\Delta\varphi = \frac{2\pi}{\lambda} (n_{\text{slow}} - n_{\text{fast}}) \cdot d, \quad (\text{A.1})$$

where λ is the wavelength of the incident light, d is the thickness of the waveplate and n_{slow} and n_{fast} corresponds to the refraction index of the slow and fast axis, respectively.

The most common types of waveplates are the *Quarter-Wave Plate* (*QWP* or $\lambda/4$ plate) and the *Half-Wave Plate* (*HWP* or $\lambda/2$ plate), where the

denomination is due to the characteristic retardation. The HWP rotates the polarization vector according to the transformation [Barnett09]

$$T_{\text{HWP}}(\theta) = \begin{pmatrix} \cos(2\theta) & \sin(2\theta) \\ \sin(2\theta) & -\cos(2\theta) \end{pmatrix} \quad (\text{A.2})$$

expressed in $\{|H\rangle, |V\rangle\}$, where the angle θ is defined as angle between $|V\rangle$ -polarization and the optical axis of the birefringent crystal. Thus, for linear polarized light this is just a rotation to another linear polarization. A QWP can change linear to circular polarization with the transformation matrix expressed in $\{|H\rangle, |V\rangle\}$ [Barnett09]

$$T_{\text{QWP}}(\theta) = \begin{pmatrix} \cos^2(\theta) - i \sin^2(\theta) & (1 - i) \sin(\theta) \cos(\theta) \\ (1 + i) \sin(\theta) \cos(\theta) & -i \cos^2(\theta) + \sin^2(\theta) \end{pmatrix}. \quad (\text{A.3})$$

By choosing the plates and their angles carefully any polarization can be transformed into any desired polarization state, which is of interest for the polarization analysis described in sec. 3.1.5.

A.1.3 Yttrium-vanadate crystals

The *Yttrium-vanadate crystal* (YVO_4 or later just *YVO*) is, just like wave-plates, a birefringent optical device for manipulation of the polarization. Its transformation matrix is given by

$$T_{\text{YVO}}(\phi) = e^{-\frac{\phi}{2}} \begin{pmatrix} 1 & 0 \\ 0 & e^{i\phi} \end{pmatrix}, \quad (\text{A.4})$$

with the effective phase ϕ , which depends on the angle by which the YVO is tilted around its optical axis. It can be seen from eq. (A.4) that the rotation causes a phase shift between horizontal and vertical polarization.

A.1.4 Beam splitter

A *beam splitter* (*BS*) is an optical device, which can split incident light in two or more beams in a balanced or unbalanced way. In this thesis ideally balanced BS with two output ports were used, so descriptions of the other cases are omitted. A scheme for a BS is depicted in fig. A.1 with A , B as

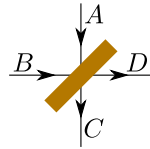


Figure A.1: **Scheme of beam splitter:** An incident beam in arm $A(B)$ is transmitted in $C(D)$ and reflected in $D(C)$.

the input ports and C , D as the output ports. An incident photon in arm A can be either transmitted in C or reflected in D , where the output port is chosen randomly. With analogous behavior for the incident beam in arm B these operation can be modeled as

$$|A\rangle \rightarrow \frac{1}{\sqrt{2}} (|C\rangle + |D\rangle) \quad (\text{A.5})$$

$$|B\rangle \rightarrow \frac{1}{\sqrt{2}} (|C\rangle - |D\rangle). \quad (\text{A.6})$$

With these equations the output port can be described by

$$|C\rangle \rightarrow \frac{1}{\sqrt{2}} (|A\rangle + |B\rangle). \quad (\text{A.7})$$

A special case for BS are the *Polarizing Beam Splitters (PBS)*, which transmit horizontal polarized light and reflect vertical polarized light.

A.1.5 Fabry-Pérot cavity

A Fabry-Pérot cavity is a linear optical interferometer consisting of two parallel, highly reflecting mirrors. For a resonator with planar mirrors the modes extend up to the edges of the mirrors, which causes diffraction losses. Because light is only transmitted for special equidistant frequencies, it is often used as spectrum analyzer. It is furthermore possible to tune the cavity length and thus change the resonance frequencies. If the tuning is done periodically, e.g. with a piezo actuator in a triangular temporal shape, the transmitted power can be monitored by a photodetector and an oscilloscope, which can display the optical spectrum of the incident light given that the spectral width is smaller than the free spectral range [Saleh91, Vaughan89].

A.2 Methods

A.2.1 Phase correction

A very important parameter for the evaluations in this thesis is the phase φ between the two arms of the interferometer. As already described in sec. 3.1.3 the phase is varied by a continuously piezo driven prism in arm B , and thus also the intensity of the interference signal over time as depicted in fig. A.2 a), which is proportional to the sum voltage of a PSD. Due to a non-linearity of the piezo the maxima/minima are not equidistant in time to the next maximum/minimum, which can be seen in fig. A.2 b). Thus, would be not possible to fit a sine function to the full temporal interference signal, from which the phase could be easily determined. To each point in time the correct phase is assigned by considering each flank of the intensity

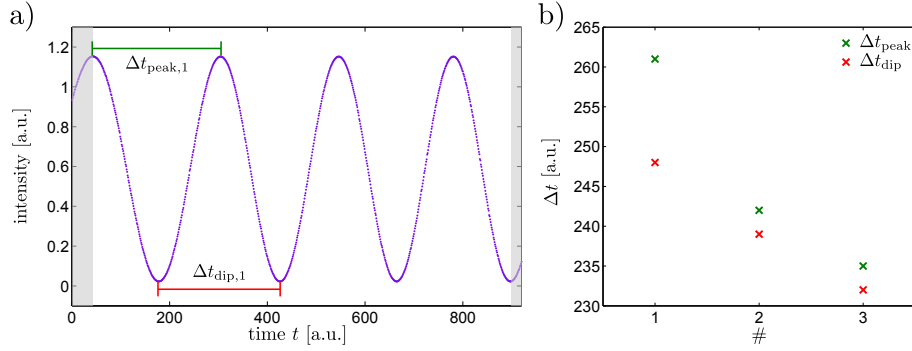


Figure A.2: **Phase correction:** a) The violet dots show a recorded interference signal over time. Because of a non-linearity of the piezo the maxima/minima are not temporal equidistant to each other, which can be seen in b). The phase can be determined by considering for each slope the relative distance of the data point to the neighboring extrema according to a arcsin-function. Hence, the signal is cut as indicated by the gray areas.

between two extrema separately. The phase is calculated from the relative distance between neighboring extrema according to a arcsin-function. Due to this procedure, the data is only taken from the first extremum to the last extremum as it is indicated by the gray areas in fig. A.2 a). The phase corrected interference signal is shown in fig. A.3.

Not all data sets taken at the same time show a sinusoidal behavior, but all share the same time stamps. Hence, to assign a certain phase to them, the time stamps are substituted by the corresponding phase, obtained by evaluating the interference signal according to the above method.

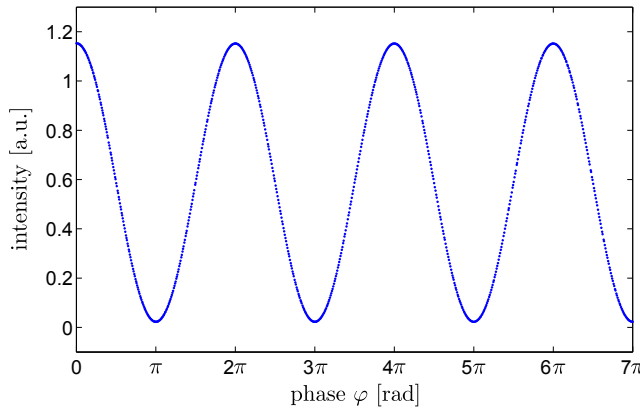


Figure A.3: **Phase corrected signal:** After the phase correction the interference signal is a perfect sinusoidal function dependent on the phase φ .

A.2.2 Estimation of position error

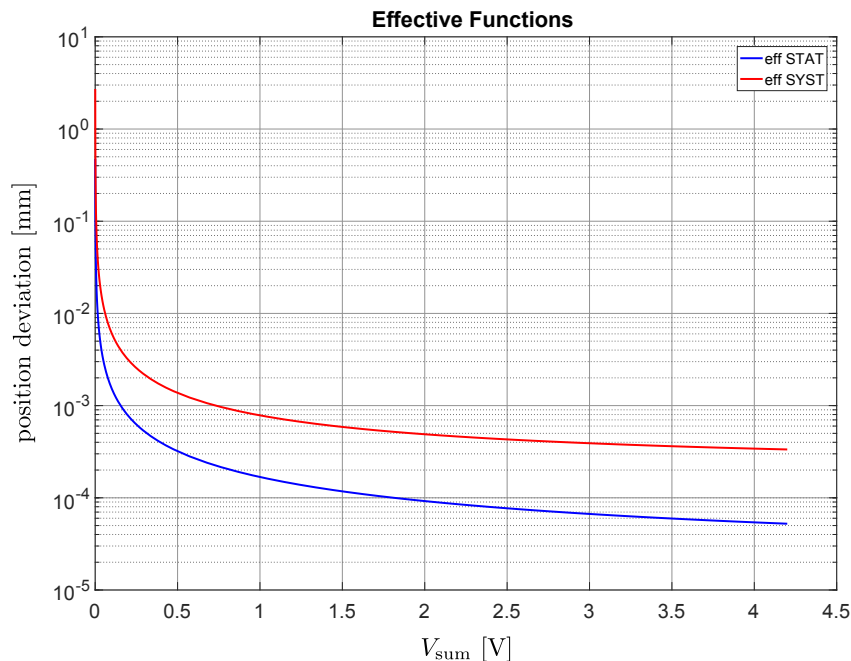


Figure A.4: **Error estimation of the position:**. The red curve shows the systematic error estimation function and the blue curve depicts the statistical error estimation function. It can be seen that the systematic error is the main factor in the constituted error. The smaller the sum voltage V_{sum} (e.g. in the case of destructive interference) the larger the impact of both error sources.

In this work the position of the beam is read out by position sensing detectors (PSDs) according to formula (3.1). To estimate the error a further measurement was performed for investigation of the behavior of the measured beam position on the PSD dependent on the sum voltage V_{sum} . For this purpose the laser power was attenuated in a controlled way and the position on the PSD was recorded for every set power several times. It could be observed that for smaller V_{sum} the read out position was shifted to the corners of the detector area. From the measured data error functions were obtained for the systematic and the statistical error, which are depicted in fig. A.4. In our measurements the sum voltage varied in the range about $0.5 \text{ V} \lesssim V_{\text{sum}} \lesssim 4.3 \text{ V}$. It can be seen from fig. A.4 that the systematic error is almost an order of magnitude bigger than the statistical error and therefore the main error source. Furthermore, from this plot it can be concluded that the interference signal for beams of almost equal intensity experience a bigger error than beams, which differ in their intensities since

almost perfect destructive IF occurs. This fact can be exploited to minimize systematic errors by choosing properly the intensity ratio of the two arms.

Appendix B

Mathematical calculations

B.1 Derivation of mixed state of the system

Let $|\Phi\rangle$, $|\Phi^\perp\rangle$, $(\psi_j)_{j \in J}$ be an orthonormal basis for the underlying Hilbert space, where J is some index set. Then

$$\begin{aligned} \text{Tr}_\Phi (|\Lambda\rangle\langle\Lambda|) &= \langle\Phi| \left[\cos\alpha |A\rangle\eta(|\Phi\rangle + \epsilon|\Phi^\perp\rangle) + \sin\alpha e^{i\varphi} |B\rangle|\Phi\rangle \right] \\ &\cdot \left[(\langle\Phi| + \epsilon\langle\Phi^\perp|)\eta\langle A| \cos\alpha + \langle\Phi|\langle B| \sin\alpha e^{-i\varphi} \right] |\Phi\rangle \end{aligned} \quad (\text{B.1})$$

$$\begin{aligned} &+ \langle\Phi^\perp|\Lambda\rangle\langle\Lambda|\Phi^\perp\rangle + \sum_{j \in J} \langle\psi_j|\Lambda\rangle\langle\Lambda|\psi_j\rangle \\ &= \cos^2\alpha \eta^2(1 + \epsilon^2) |A\rangle\langle A| + \cos\alpha \sin\alpha e^{-i\varphi} |A\rangle\langle B| \\ &+ \cos\alpha \sin\alpha e^{i\varphi} |B\rangle\langle A| + \sin^2\alpha |B\rangle\langle B| + 0, \end{aligned} \quad (\text{B.2})$$

where the sum over J vanishes due to orthogonality of the basis vectors. By the definition of η we obtain $\eta^2(1 + \epsilon^2) = 1$, hence the above expression can be rewritten as matrix acting on the two-dimensional vector space spanned by $|A\rangle$ and $|B\rangle$ via

$$\rho_I = \text{Tr}_\Phi (|\Lambda\rangle\langle\Lambda|) = \begin{pmatrix} \cos^2\alpha & \cos\alpha \sin\alpha e^{-i\varphi}\eta \\ \cos\alpha \sin\alpha e^{i\varphi}\eta & \sin^2\alpha \end{pmatrix}. \quad (\text{B.3})$$

B.2 Derivation of the state of postselected external systems (omitting normalization)

$$\langle \Psi_I | \Lambda \rangle = \left(\frac{1}{\sqrt{2}} (\langle A | + \langle B |) \right) \cdot (\cos \alpha |A\rangle | \Phi' \rangle + \sin \alpha e^{i\varphi} |B\rangle | \Phi \rangle) \quad (\text{B.4})$$

$$= \frac{1}{\sqrt{2}} (\cos \alpha | \Phi' \rangle + \sin \alpha e^{i\varphi} | \Phi \rangle) \quad (\text{B.5})$$

$$= \frac{1}{\sqrt{2}} \left(\cos \alpha \left(\eta (| \Phi \rangle + \epsilon | \Phi^\perp \rangle) \right) + \sin \alpha e^{i\varphi} | \Phi \rangle \right) \quad (\text{B.6})$$

$$= \frac{1}{\sqrt{2}} \left[| \Phi \rangle + \frac{\cos \alpha \eta \epsilon}{\cos \alpha \eta + \sin \alpha e^{i\varphi}} | \Phi^\perp \rangle \right] \quad (\text{B.7})$$

$$= \frac{1}{\sqrt{2}} \left[| \Phi \rangle + \frac{\eta \epsilon}{\eta + \tan \alpha e^{i\varphi}} | \Phi^\perp \rangle \right] \quad (\text{B.8})$$

with the assumption that $(\cos \alpha \eta + \sin \alpha e^{i\varphi}) \neq 0$ from eq. (B.6) to (B.7).

B.3 Derivation of the shifts of expectation values

The shift in the expectation value for an operator \hat{O} is derived with the ansatz of eq. (4.1).

$$\mathcal{D}(O) \equiv \langle \Phi' | \hat{O} | \Phi' \rangle - \langle \Phi | \hat{O} | \Phi \rangle \quad (\text{B.9})$$

$$= \eta^2 \left(\langle \Phi | \hat{O} | \Phi \rangle + \epsilon \langle \Phi | \hat{O} | \Phi^\perp \rangle + \epsilon \langle \Phi^\perp | \hat{O} | \Phi \rangle + \epsilon^2 \langle \Phi^\perp | \hat{O} | \Phi^\perp \rangle \right) - \langle \Phi | \hat{O} | \Phi \rangle \quad (\text{B.10})$$

= ...

With the Taylor expansion $\eta^2 = 1 - \epsilon^2 + \mathcal{O}(\epsilon^4)$ for $\epsilon \ll 1$ we get

$$\dots = \langle \Phi | \hat{O} | \Phi \rangle + 2\epsilon \text{Re} \left[\langle \Phi | \hat{O} | \Phi^\perp \rangle \right] + \mathcal{O}(\epsilon^2) - \langle \Phi | \hat{O} | \Phi \rangle \quad (\text{B.11})$$

$$= 2\epsilon \text{Re} \left[\langle \Phi | \hat{O} | \Phi^\perp \rangle \right] + \mathcal{O}(\epsilon^2). \quad (\text{B.12})$$

B.4 Derivation of $|\Phi'_j\rangle$

We want to derive formula (4.1) for a single external system j . For that purpose we consider explicitly the weak interaction ($\Gamma_j \ll 1$) generated by the indicator $\hat{\mathbf{B}}$ on the single the pointer system $|\Phi_j\rangle$

$$|\Phi'_j\rangle = e^{-i\Gamma\hat{\mathbf{B}}} |\Phi_j\rangle \quad (\text{B.13})$$

$$\approx (1 - i\Gamma\hat{\mathbf{B}}) |\Phi_j\rangle. \quad (\text{B.14})$$

The orthogonal component of eq. (4.1) can be calculated by using the Gram-Schmidt process

$$|\Phi_j^\perp\rangle = \mathcal{N} (|\Phi_j'\rangle - \langle\Phi_j|\Phi_j'\rangle|\Phi_j\rangle) \quad (\text{B.15})$$

$$\approx \mathcal{N} i\Gamma \left(\langle\hat{\mathbf{B}}\rangle_0 - \hat{\mathbf{B}} \right) |\Phi_j\rangle \quad (\text{B.16})$$

with $\langle\hat{\mathbf{B}}\rangle_0$ denoting the initial expectation value of the observable and with \mathcal{N} denoting the normalization factor, which is given by

$$\mathcal{N}^{-1} = \Gamma \Delta B. \quad (\text{B.17})$$

Considering a general global phase we obtain for $|\Phi_j^\perp\rangle$

$$|\Phi_j^\perp\rangle \equiv e^{i\beta} \frac{\hat{\mathbf{B}} - \langle\hat{\mathbf{B}}\rangle_0}{\Delta B}. \quad (\text{B.18})$$

This equation can be used by a simple rearrangement to evaluate $\hat{\mathbf{B}}|\Phi_j\rangle$ in eq. (B.14), which then yields

$$|\Phi_j'\rangle \approx |\Phi_j\rangle - i\Gamma \left(\langle\hat{\mathbf{B}}\rangle_0 |\Phi_j\rangle e^{-i\beta} \Delta B |\Phi_j^\perp\rangle \right) \quad (\text{B.19})$$

$$= \left(1 - i\Gamma \langle\hat{\mathbf{B}}\rangle_0 \right) |\Phi_j\rangle - i\Gamma e^{-i\beta} \Delta B |\Phi_j^\perp\rangle \quad (\text{B.20})$$

$$\approx |\Phi_j\rangle - i\Gamma e^{-i\beta} \Delta B |\Phi_j^\perp\rangle \quad (\text{B.21})$$

$$= |\Phi_j\rangle - \epsilon_j |\Phi_j^\perp\rangle \quad (\text{B.22})$$

with the assumption that $\langle\hat{\mathbf{B}}\rangle_0 \approx 0$ and the definition $\epsilon_j \equiv -i\Gamma e^{-i\beta} \Delta B$. By choosing the phase β properly we obtain a real $\epsilon_j > 0$.

B.5 Derivation of expectation values of complementary observables

In this section the expectation values for complementary observables (eq. (4.26) and (4.27)) are derived for a single external system with the results of the previous section B.4. The pointer shift is calculated according to the definition (4.24) with the postselected density matrix of a single external systems given by (4.21). For the calculation of the shift in the expectation value the following expressions have to be evaluated, for which we require

that $\langle [\hat{\mathbf{B}}, \hat{\mathbf{C}}] \rangle_0 = i$, $\langle \{\hat{\mathbf{B}}, \hat{\mathbf{C}}\} \rangle_0 = 0$ and $\langle \hat{\mathbf{C}} \rangle_0 \langle \hat{\mathbf{B}} \rangle_0 = 0$

$$e^{-i\beta} \langle \Phi_j | \hat{\mathbf{B}} | \Phi_j^\perp \rangle = \Delta B \quad (\text{B.23})$$

$$e^{-i\beta} \langle \Phi_j | \hat{\mathbf{C}} | \Phi_j^\perp \rangle = \frac{\langle \hat{\mathbf{C}} \hat{\mathbf{B}} \rangle_0}{\Delta B} - \frac{\langle \hat{\mathbf{C}} \rangle_0 \langle \hat{\mathbf{B}} \rangle_0}{\Delta B} \quad (\text{B.24})$$

$$= \frac{1}{\Delta B} \left(\frac{\langle [\hat{\mathbf{B}}, \hat{\mathbf{C}}] \rangle_0}{2} + \frac{\langle \{\hat{\mathbf{B}}, \hat{\mathbf{C}}\} \rangle_0}{2} \right) - \frac{\langle \hat{\mathbf{C}} \rangle_0 \langle \hat{\mathbf{B}} \rangle_0}{\Delta B} \quad (\text{B.25})$$

$$= \frac{i}{2\Delta B}. \quad (\text{B.26})$$

Furthermore the expectation values of the interacted pointer state have to be determined

$$\langle \Phi'_j | \hat{\mathbf{B}} | \Phi'_j \rangle = \langle \hat{\mathbf{B}} \rangle_0 \quad (\text{B.27})$$

$$\langle \Phi'_j | \hat{\mathbf{C}} | \Phi'_j \rangle = \langle \hat{\mathbf{C}} \rangle_0 + \Gamma. \quad (\text{B.28})$$

With these results the expectation value of the pre- and postselected system for the observables $\hat{\mathbf{C}}$ and $\hat{\mathbf{B}}$ can be calculated

$$\text{Tr}(\hat{\mathbf{B}}\rho_j) \approx \langle \Phi_j | \hat{\mathbf{B}} | \Phi_j \rangle + 2 \text{Re} \left[-i\Gamma \Delta B (P_A)_w e^{-i\beta} \langle \Phi_j | \hat{\mathbf{B}} | \Phi_j^\perp \rangle \right] \quad (\text{B.29})$$

$$= \langle \hat{\mathbf{B}} \rangle_0 + 2\Gamma(\Delta B)^2 \text{Re}[-i(P_A)_w] \quad (\text{B.30})$$

$$= \langle \hat{\mathbf{B}} \rangle_0 + 2\Gamma(\Delta B)^2 \text{Im}[(P_A)_w] \quad (\text{B.31})$$

$$\text{Tr}(\hat{\mathbf{C}}\rho_j) \approx \langle \Phi_j | \hat{\mathbf{C}} | \Phi_j \rangle + 2 \text{Re} \left[-i\Gamma \Delta B (P_A)_w e^{-i\beta} \langle \Phi_j | \hat{\mathbf{C}} | \Phi_j^\perp \rangle \right] \quad (\text{B.32})$$

$$= \langle \hat{\mathbf{C}} \rangle_0 + \Gamma \text{Re}[(P_A)_w]. \quad (\text{B.33})$$

Finally we obtain for the shifts in the expectation values (according to (4.24))

$$\mathcal{D}_F(\hat{\mathbf{B}}) \approx 2\Gamma(\Delta B)^2 \text{Im}[(P_A)_w] \quad (\text{B.34})$$

$$\mathcal{D}_F(\hat{\mathbf{C}}) \approx \Gamma \text{Re}[(P_A)_w]. \quad (\text{B.35})$$

B.6 Analysis of validity of expectation value expressions for strong interactions

This proof is due to Jan Dziewior, who is one of the authors of [Dziewior18].

In this section the conditions are analyzed under which the standard expressions for the shifts of the expectation values (4.37) and (4.38) cease to be approximations and obtain validity for interactions of arbitrary strength. This analysis considers the general case of arbitrary pre- and postselected systems and derives general conditions for pointer states under which the expressions are exact. For clarity all tensor products are explicitly denoted by the symbol \otimes .

The relevant state space can be divided into two parts, the space of the analyzed pointer \mathcal{H}_P , and the space of the pre- and postselected system \mathcal{H}_S . We consider an arbitrary forward evolving state ρ_0 and a general postselection parametrized by the quantum operation $\hat{\mathbf{M}} = \hat{\mathbf{E}}^\dagger \hat{\mathbf{E}}$ acting on \mathcal{H}_S . Prior to the interaction the pointer is in the state γ_0 . Note, that since we allow partial pre- and postselection, \mathcal{H}_S can be arbitrary large and contain any portion of the environment as well. This scenario is most general and contains all special cases usually discussed in the context of weak values.

The presented theorem is valid under three conditions. (1) Initially the relevant pointer is not entangled with the other systems, such that the initial composite state χ_0 can be expressed as

$$\chi_0 = \rho_0 \otimes \gamma_0. \quad (\text{B.36})$$

This means that the pointer is a suitable measurement device in the standard framework of quantum measurement. (2) The pointer system interacts with systems in the considered Hilbert space \mathcal{H}_S only. This interaction is an unitary evolution $\hat{\mathbf{U}}_I$ can be parametrized as

$$\hat{\mathbf{U}}_I = e^{-ig\hat{\mathbf{A}} \otimes \hat{\mathbf{K}}}, \quad (\text{B.37})$$

where the operator $\hat{\mathbf{A}}$ acts on \mathcal{H}_S and $\hat{\mathbf{K}}$ acts on \mathcal{H}_P . The parameter $g \geq 0$ represents the effective strength of the interaction. (3) During the time interval where the pointer system interacts with the pre- and postselected system, all other evolutions of the latter commute with this interaction at each point in time. This implies that the final state is independent of the specific time ordering of the two types of evolution and consequently, the remaining evolution of the system can be expressed by a single effective operator $\hat{\mathbf{U}}_S$, which commutes with $\hat{\mathbf{U}}_I$. The total evolution of system and pointer \mathbf{U}_T can be expressed by a product of the two types of evolution as

$$\hat{\mathbf{U}}_T = \hat{\mathbf{U}}_I \hat{\mathbf{U}}_S = \hat{\mathbf{U}}_S \hat{\mathbf{U}}_I. \quad (\text{B.38})$$

Since both $\hat{\mathbf{U}}_S$ and $\hat{\mathbf{U}}_I$ commute with $\hat{\mathbf{A}}$, the weak value of $\hat{\mathbf{A}}$ is constant over the whole interval of this interaction and can be calculated at any point in time therein. Thus, if condition (3) is satisfied we can calculate the weak value without the loss of generality at any time during the interaction.

Under the presented conditions the composite state of all systems after postselection χ_F can be written as

$$\chi_F = \mathcal{N} \hat{\mathbf{E}} \hat{\mathbf{U}}_I \hat{\mathbf{U}}_S \chi_0 \hat{\mathbf{U}}_S^\dagger \hat{\mathbf{U}}_I^\dagger \hat{\mathbf{E}}^\dagger, \quad (\text{B.39})$$

with the normalization factor

$$\mathcal{N}^{-1} = \text{Tr} \left(\hat{\mathbf{E}} \hat{\mathbf{U}}_I \hat{\mathbf{U}}_S \chi_0 \hat{\mathbf{U}}_S^\dagger \hat{\mathbf{U}}_I^\dagger \hat{\mathbf{E}}^\dagger \right). \quad (\text{B.40})$$

The idea of this analysis is to compare the final pointer state $\gamma_F = \text{Tr}_S(\chi_F)$ with the weak value calculated for this pre- and postselected system with respect to the operator $\hat{\mathbf{A}}$. This comparison then implies conditions under which the weak value correctly describes the amplification of the shift of the expectation values.

B.6.1 Expectation Values of Final Pointer State

We start by considering the expectation value of an arbitrary observable \mathbf{O} for the final state of the pointer γ_F . Expanding the interaction $\hat{\mathbf{U}}_I$ in orders of g this expectation value can be written as

$$\text{Tr}(\gamma_F \hat{\mathbf{O}}) = \text{Tr}(\chi_F \hat{\mathbf{O}}) \quad (\text{B.41})$$

$$= \mathcal{N} \text{Tr}(\hat{\mathbf{E}} \hat{\mathbf{U}}_I \hat{\mathbf{U}}_S \chi_0 \hat{\mathbf{U}}_S^\dagger \hat{\mathbf{U}}_I^\dagger \hat{\mathbf{E}}^\dagger \hat{\mathbf{O}}) \quad (\text{B.42})$$

$$= \mathcal{N} \sum_{n,m} \frac{(-1)^n i^{m+n}}{m! n!} g^{m+n} \text{Tr}(\mathbf{K}^n \mathbf{O} \mathbf{K}^m \gamma_0) \text{Tr}(\mathbf{E} \mathbf{A}^m \mathbf{U}_S \chi_0 \mathbf{U}_S^\dagger \mathbf{A}^n \mathbf{E}^\dagger) \quad (\text{B.43})$$

$$= \mathcal{N} \sum_{n,m} \frac{(-1)^n i^{m+n}}{m! n!} g^{m+n} A_{mn} \text{Tr}(\hat{\mathbf{K}}^n \hat{\mathbf{O}} \hat{\mathbf{K}}^m \gamma_0), \quad (\text{B.44})$$

where A_{mn} is complex number with

$$A_{mn} \equiv \text{Tr}(\hat{\mathbf{E}} \hat{\mathbf{A}}^m \hat{\mathbf{U}}_S \chi_0 \hat{\mathbf{U}}_S^\dagger \hat{\mathbf{A}}^n \hat{\mathbf{E}}^\dagger). \quad (\text{B.45})$$

B.6.2 Calculation of Weak Value

As discussed above we choose without loss of generality to calculate the weak value at the begin of the interaction. The forward evolving state χ_1 can then be written as

$$\chi_1 = \chi_0. \quad (\text{B.46})$$

The backward evolving operator χ_2 is obtained by applying the evolution operators backwards to the postselection $\hat{\mathbf{M}} = \hat{\mathbf{E}}^\dagger \hat{\mathbf{E}}$ operator as

$$\chi_2 = \hat{\mathbf{U}}_S^\dagger \hat{\mathbf{U}}_I^\dagger \hat{\mathbf{E}} \hat{\mathbf{U}}_I \hat{\mathbf{U}}_S. \quad (\text{B.47})$$

The weak value of operator $\hat{\mathbf{A}}$ becomes

$$A_w = \frac{\text{Tr}(\chi_2 \hat{\mathbf{A}} \chi_1)}{\text{Tr}(\chi_2 \chi_1)} \quad (\text{B.48})$$

$$= \frac{\text{Tr}(\hat{\mathbf{U}}_S^\dagger \hat{\mathbf{U}}_I^\dagger \hat{\mathbf{E}}^\dagger \hat{\mathbf{E}} \hat{\mathbf{U}}_I \hat{\mathbf{U}}_S \hat{\mathbf{A}} \chi_0)}{\text{Tr}(\hat{\mathbf{U}}_S^\dagger \hat{\mathbf{U}}_I^\dagger \hat{\mathbf{E}}^\dagger \hat{\mathbf{E}} \hat{\mathbf{U}}_I \hat{\mathbf{U}}_S \chi_0)} \quad (\text{B.49})$$

$$= \mathcal{N} \text{Tr}(\hat{\mathbf{E}} \hat{\mathbf{A}} \hat{\mathbf{U}}_I \hat{\mathbf{U}}_S \chi_0 \hat{\mathbf{U}}_S^\dagger \hat{\mathbf{U}}_I^\dagger \hat{\mathbf{E}}^\dagger). \quad (\text{B.50})$$

Please note, how from the form of expression (B.49) it becomes immediately clear that the weak value can be computed at any time between pre- and postselection as long as assumption (3) is valid and it commutes with all evolutions.

To express the weak value in the same form as (B.44) we use assumption (3) and expand it in orders of g to

$$A_w = \mathcal{N} \sum_{n,m=0} \frac{(-1)^n i^{m+n}}{m! n!} g^{m+n} \text{Tr}(\gamma_0 \hat{\mathbf{K}}^{m+n}) \text{Tr}(\hat{\mathbf{E}} \hat{\mathbf{A}}^{m+1} \hat{\mathbf{U}}_S \chi_0 \hat{\mathbf{U}}_S^\dagger \hat{\mathbf{A}}^n \hat{\mathbf{E}}^\dagger) \quad (\text{B.51})$$

$$= \mathcal{N} \frac{i}{g} \sum_{n,m=0} (m+1) \frac{(-1)^n i^{m+n+1}}{(m+1)! n!} g^{m+n+1} \text{Tr}(\gamma_0 \hat{\mathbf{K}}^{m+n})$$

$$\text{Tr}(\hat{\mathbf{E}} \hat{\mathbf{A}}^{m+1} \hat{\mathbf{U}}_S \chi_0 \hat{\mathbf{U}}_S^\dagger \hat{\mathbf{A}}^n \hat{\mathbf{E}}^\dagger) \quad (\text{B.52})$$

$$= \mathcal{N} \frac{i}{g} \sum_{n,m=0} m \frac{(-1)^n i^{m+n}}{m! n!} g^{m+n} A_{mn} \text{Tr}(\gamma_0 \hat{\mathbf{K}}^{m+n-1},) \quad (\text{B.53})$$

where in the last line the summation over a summand with the factor $m = 0$ has been added.

This expression can now be inserted in the formulas for the expectation values with

$$\delta X = g \text{Re}[A_w] \quad (\text{B.54})$$

$$\delta K = 2g(\Delta K)^2 \text{Im}[A_w]. \quad (\text{B.55})$$

B.6.3 Comparison of Expressions

Since it holds that $A_{mn}^* = A_{nm}$ we compare pairs of expression from the two sums that contain A_{mn} and A_{nm} . Combining the real part expression (B.54) with the expression for the expectation value of $\hat{\mathbf{O}} = \hat{\mathbf{X}}$ (B.44) yields

the two conditions

$$\operatorname{Re} \left[\operatorname{Tr} \left(\gamma_0 \hat{\mathbf{K}}^p \hat{\mathbf{X}} \right) \right] = \operatorname{Tr} \left(\gamma_0 \hat{\mathbf{X}} \right) \operatorname{Tr} \left(\gamma_0 \hat{\mathbf{K}}^p \right), \quad (\text{B.56})$$

$$\operatorname{Im} \left[\operatorname{Tr} \left(\gamma_0 \hat{\mathbf{K}}^p \hat{\mathbf{X}} \right) \right] = -\frac{p}{2} \operatorname{Tr} \left(\gamma_0 \hat{\mathbf{K}}^{p-1} \right), \quad (\text{B.57})$$

where it has been used that for the complementary observables \mathbf{X} and $\hat{\mathbf{K}}$ it holds that

$$\operatorname{Tr} (\gamma_0 \mathbf{K}^n \mathbf{X} \mathbf{K}^m) = \operatorname{Tr} (\gamma_0 \mathbf{K}^{m+n} \mathbf{X}) + im \operatorname{Tr} (\gamma_0 \mathbf{K}^{m+n-1}). \quad (\text{B.58})$$

From the equality of the expression for the imaginary part (B.55) and the expectation where $\mathbf{O} = \mathbf{K}$ we arrive at the single condition

$$\operatorname{Tr} (\gamma_0 \mathbf{K}^{p+1}) = \operatorname{Tr} (\gamma_0 \mathbf{K}) \operatorname{Tr} (\gamma_0 \mathbf{K}^p) + 2(\Delta K)^2 \operatorname{Tr} (\gamma_0 \mathbf{K}^{p-1}). \quad (\text{B.59})$$

The set of equations (B.56), (B.57) and (B.59) represents the necessary and sufficient conditions that the initial pointer state γ_0 has to satisfy with respect to the operators \mathbf{X} and \mathbf{K} .

B.7 Expectation values for Gaussian states

The spatial Gaussian state is given by the expression

$$\Phi(x) = \left(\frac{1}{2\pi\sigma^2} \right)^{\frac{1}{4}} e^{-\frac{(x-x_0)}{4\sigma^2}} e^{ip_0x}, \quad (\text{B.60})$$

where x_0 denotes the initial position, p_0 the initial momentum, and σ denotes the uncertainty. Remember that we consider the calculations for $\hbar = 1$. The Gaussian state in momentum representation can be derived by a Fourier transform

$$\tilde{\Phi}(p) = \left(\frac{2\pi\sigma^2}{\pi} \right)^{\frac{1}{4}} e^{-(k-k_0)\sigma^2} e^{-i(p-p_0)x_0}. \quad (\text{B.61})$$

The twofold expectation value, which is required in sec. 5.2.1, can be considered with the Gaussian state and the spatial operator $\hat{\mathbf{x}}$ in the momentum representation, $\hat{\mathbf{x}} = i\partial/\partial\hat{\mathbf{p}}$

$$\langle \hat{\mathbf{p}}^k \hat{\mathbf{x}} \rangle = \langle \hat{\mathbf{p}}^k i \frac{\partial}{\partial \hat{\mathbf{p}}} \rangle. \quad (\text{B.62})$$

The calculation of the derivation yields

$$\frac{\partial}{\partial \hat{\mathbf{p}}} \tilde{\Phi}(p) = -(k-k_0)\sigma^2 - ix_0 \tilde{\Phi}(p), \quad (\text{B.63})$$

with $\sigma^2 = (\Delta p)^{-2}/2$. By inserting this to the above eq. we obtain the required expression

$$\langle \hat{\mathbf{p}}^k \hat{\mathbf{x}} \rangle = -\frac{i}{2(\Delta p)^2} \left(\langle \hat{\mathbf{p}}^{k+1} \rangle - \langle \hat{\mathbf{p}} \rangle \langle \hat{\mathbf{p}}^k \rangle \right) + \langle \hat{\mathbf{x}} \rangle \langle \hat{\mathbf{p}}^k \rangle. \quad (\text{B.64})$$

B.8 Derivation of the fit formula

For the derivation of the fit formula we start with the paraxial approximation of eq. (5.20)

$$r_x \approx \mathcal{D}_F(x) + z \frac{\mathcal{D}_F(p_x)}{|\vec{p}|}$$

where z denotes the detector position and $|\vec{p}|$ the total momentum with $|\vec{p}| = 2\pi/\lambda$ (whereby $\hbar = 1$ and λ as the wavelength of the photons). Inserting the exact formulas for the shift of the expectation values after the postselection (eq. (4.37) and eq. (4.38)) into the above formula we obtain

$$r_x \approx \delta x \operatorname{Re} [(P_A)_w] - 2\delta p_x (\Delta x)^2 \operatorname{Im} [(P_A)_w] + \frac{z}{|\vec{p}|} \left(\delta p_x \operatorname{Re} [(P_A)_w] + \frac{\delta x}{2(\Delta x)^2} \operatorname{Im} [(P_A)_w] \right).$$

Using the uncertainty of a Gaussian beam eq. (5.1)

$$(\Delta x)^2 = \frac{w_0^2}{4} = z_R \frac{\lambda}{4\pi}$$

and the paraxial approximation for the momentum eq. (4.45) for the respective degree of freedom

$$\delta p_x = \frac{2\pi}{\lambda} \delta \theta_x,$$

yields

$$r_x \approx \delta x \operatorname{Re} [(P_A)_w] - 2 \frac{2\pi}{\lambda} \delta \theta_x z_R \frac{\lambda}{4\pi} \operatorname{Im} [(P_A)_w] + \frac{z}{\frac{2\pi}{\lambda}} \left(\frac{2\pi}{\lambda} \delta \theta_x \operatorname{Re} [(P_A)_w] + \frac{\delta x}{2z_R \frac{\lambda}{4\pi}} \operatorname{Im} [(P_A)_w] \right) \quad (\text{B.65})$$

$$= \delta x \operatorname{Re} [(P_A)_w] - z_R \delta \theta_x \operatorname{Im} [(P_A)_w] + z \delta \theta_x \operatorname{Re} [(P_A)_w] + \frac{z}{z_R} \delta x \operatorname{Im} [(P_A)_w]. \quad (\text{B.66})$$

By rearranging eq. (B.66) we obtain the final fit function eq. (5.22)

$$r_x \approx \delta x \left(\operatorname{Re} [(P_A)_w] + \frac{z}{z_R} \operatorname{Im} [(P_A)_w] \right) + z_R \delta \theta_x \left(\frac{z}{z_R} \operatorname{Re} [(P_A)_w] - \operatorname{Im} [(P_A)_w] \right).$$

Acknowledgments

First of all, I want to thank Prof. Dr. Harald Weinfurter for the opportunity to do my Master thesis in his group. I am very grateful for his advices and support during the whole time, and especially for his great efforts in the last steps of my thesis.

A special thanks also to Jan Dziejwior and Lukas Knips, who helped me whenever they could in any concerns – no matter whether it was about explaining the theory or active support at the experiments, about the corrections or the figures of this work, or simply about having amusing discussions at lunch.

I also want to thank Lev Vaidman for the collaboration and his efforts for the project, which my master thesis is based on. Furthermore, I am grateful to everyone, who corrected my thesis and thus helped me to improve it.

A special thanks to Dennis Gallenmüller, not only for the fruitful mathematical discussions and the helpful advices concerning the thesis but also for his support during the whole time. To the whole group, the people in Garching and downtown, thank you for making me feel welcome and having a good time.

I also want to say thanks to everyone else, who supported me in any kind of way. Zu guter Letzt möchte ich mich insbesondere auch bei meinen Eltern bedanken, die mich während meines gesamten Studiums und darüber hinaus unterstützt haben.

List of Figures

2.1	Von Neumann measurement model	5
2.2	Scheme of pre- and postselected measurement	8
2.3	Von Neumann scheme for PPS measurement	8
2.4	Comparison standard measurement with PPS measurement	11
3.1	Experimental setup	13
3.2	Bloch sphere	16
3.3	Geometrical scheme to derive angular and spatial deviation	17
3.4	Geometrical considerations about how to set a displacement and angle with two tilting angles	18
4.1	Comparison of the effect of various interactions in a single-path system and in a MZI	22
4.2	Parameter dependence of the modified weak value	29
4.3	Interferometer setup for demonstrating the universality and the parameter dependence of the modified weak value	30
4.4	Interference signal dependent on phase	33
4.5	Observation of universality	34
4.6	Modification of weak value due to loss of coherence	36
5.1	Alignment procedure	46
A.1	Scheme of beam splitter	54
A.2	Phase correction	56
A.3	Phase corrected signal	56
A.4	Error estimation	57

List of Tables

4.1	Summary of interactions	32
5.1	Obtained misalignment parameters	45

Bibliography

- [Abbott16] ABBOTT, B.P.; ABBOTT, R.; ABBOTT, T.; ABERNATHY, M.; ACERNESE, F.; ACKLEY, K.; ADAMS, C.; ADAMS, T.; ADDESSO, P.; ADHIKARI, R. ET AL. ‘Observation of gravitational waves from a binary black hole merger.’ In: *Physical review letters*, volume 116(6):061102 (2016).
- [Aharonov64] AHARONOV, Y.; BERGMANN, P.G. AND LEBOWITZ, J.L. ‘Time symmetry in the quantum process of measurement.’ In: *Physical Review*, volume 134(6B):B1410 (1964).
- [Aharonov88] AHARONOV, Y.; ALBERT, D.Z. AND VAIDMAN, L. ‘How the result of a measurement of a component of the spin of a spin-1/2 particle can turn out to be 100.’ In: *Physical review letters*, volume 60(14):1351 (1988).
- [Aharonov90] AHARONOV, Y. AND VAIDMAN, L. ‘Properties of a quantum system during the time interval between two measurements.’ In: *Phys. Rev. A*, volume 41:11–20 (Jan 1990).
- [Aharonov91] AHARONOV, Y. AND VAIDMAN, L. ‘Complete description of a quantum system at a given time.’ In: *Journal of Physics A: Mathematical and General*, volume 24(10):2315 (1991).
- [Aharonov02] AHARONOV, Y.; BOTERO, A.; POPESCU, S.; REZNIK, B. AND TOLLAKSEN, J. ‘Revisiting hardy’s paradox: counterfactual statements, real measurements, entanglement and weak values.’ In: *Physics Letters A*, volume 301(3-4):130–138 (2002).
- [Aharonov08] AHARONOV, Y. AND VAIDMAN, L. ‘The two-state vector formalism: an updated review.’ In: ‘Time in quantum mechanics,’ pp. 399–447. Springer (2008).

- [Anderson94] ANDERSON, R.; BILGER, H. AND STEDMAN, G.E. “sagnac” effect: A century of earth-rotated interferometers.’ In: *American Journal of Physics*, volume 62(11):975–985 (1994).
- [Barnett09] BARNETT, S.M. AND CROKE, S. ‘Quantum state discrimination.’ In: *Advances in Optics and Photonics*, volume 1(2):238–278 (2009).
- [Ben-Israel17] BEN-ISRAEL, A.; KNIPS, L.; DZIEWIOR, J.; MEINECKE, J.; DANAN, A.; WEINFURTER, H. AND VAIDMAN, L. ‘An improved experiment to determine the ‘past of a particle’ in the nested mach–zehnder interferometer.’ In: *Chinese Physics Letters*, volume 34(2):020301 (2017).
- [Benshalom17] BENSHALOM, N. *Quantum weak values in classical interferometry*. Master’s thesis, Tel Aviv University, School of Physics and Astronomy (2017).
- [Chen18] CHEN, G.; AHARON, N.; SUN, Y.N.; ZHANG, Z.H.; ZHANG, W.H.; HE, D.Y.; TANG, J.S.; XU, X.Y.; KEDEM, Y.; LI, C.F. ET AL. ‘Heisenberg-scaling measurement of the single-photon kerr non-linearity using mixed states.’ In: *Nature communications*, volume 9(1):93 (2018).
- [Danan13] DANAN, A.; FARFURNIK, D.; BAR-AD, S. AND VAIDMAN, L. ‘Asking photons where they have been.’ In: *Physical review letters*, volume 111(24):240402 (2013).
- [Dirac58] DIRAC, P.A.M. *The Principles of Quantum Mechanics*. Oxford University Press (1958).
- [Dixon09] DIXON, P.B.; STARLING, D.J.; JORDAN, A.N. AND HOWELL, J.C. ‘Ultrasensitive beam deflection measurement via interferometric weak value amplification.’ In: *Physical review letters*, volume 102(17):173601 (2009).
- [Dressel14] DRESSEL, J.; MALIK, M.; MIATTO, F.M.; JORDAN, A.N. AND BOYD, R.W. ‘Colloquium: Understanding quantum weak values: Basics and applications.’ In: *Reviews of Modern Physics*, volume 86(1):307 (2014).
- [Duck89] DUCK, I.; STEVENSON, P.M. AND SUDARSHAN, E. ‘The sense in which a” weak measurement” of a spin-

- 1/2 particle's spin component yields a value 100.' In: *Physical Review D*, volume 40(6):2112 (1989).
- [Dziewior18] DZIEWIOR, J.; KNIPS, L.; FARFURNIK, D.; SENKALLA, K.; BENSALOM, N.; EFRONI, J.; MEINECKE, J.; BAR-AD, S.; WEINFURTER, H. AND VAIDMAN, L. 'Universal description of local interactions and its application for interferometric alignment.' In: *in preparation* (2018).
- [Farfurnik13] FARFURNIK, D. *Weak value analysis of an optical Mach-Zehnder interferometer*. Master's thesis, Tel Aviv University, School of Physics and Astronomy (2013).
- [Feizpour11] FEIZPOUR, A.; XING, X. AND STEINBERG, A.M. 'Amplifying single-photon nonlinearity using weak measurements.' In: *Physical review letters*, volume 107(13):133603 (2011).
- [Ferrie14] FERRIE, C. AND COMBES, J. 'Weak value amplification is suboptimal for estimation and detection.' In: *Physical review letters*, volume 112(4):040406 (2014).
- [Fu15] FU, L.; HASHMI, F.; JUN-XIANG, Z. AND SHI-YAO, Z. 'An ideal experiment to determine the 'past of a particle' in the nested mach-zehnder interferometer.' In: *Chinese Physics Letters*, volume 32(5):050303 (2015).
- [Griffiths84] GRIFFITHS, R.B. 'Consistent histories and the interpretation of quantum mechanics.' In: *Journal of Statistical Physics*, volume 36(1-2):219–272 (1984).
- [Hallaji17] HALLAJI, M.; FEIZPOUR, A.; DMOCHOWSKI, G.; SINCLAIR, J. AND STEINBERG, A.M. 'Weak-value amplification of the nonlinear effect of a single photon.' In: *Nature Physics*, volume 13(6):540 (2017).
- [Hecht87] HECHT, E. *Optik*. McGraw-Hill (1987).
- [Hosten08] HOSTEN, O. AND KWIAT, P. 'Observation of the spin hall effect of light via weak measurements.' In: *Science*, volume 319(5864):787–790 (2008).
- [Knee13] KNEE, G.C.; BRIGGS, G.A.D.; BENJAMIN, S.C. AND GAUGER, E.M. 'Quantum sensors based on

- weak-value amplification cannot overcome decoherence.’ In: *Physical Review A*, volume 87(1):012115 (2013).
- [Knee14] KNEE, G.C. AND GAUGER, E.M. ‘When amplification with weak values fails to suppress technical noise.’ In: *Physical Review X*, volume 4(1):011032 (2014).
- [Kneubühl08] KNEUBÜHL, F.K. AND SIGRIST, M.W. *Laser*. Springer-Verlag (2008).
- [Kobayashi14] KOBAYASHI, H.; NONAKA, K. AND SHIKANO, Y. ‘Stereographical visualization of a polarization state using weak measurements with an optical-vortex beam.’ In: *Physical Review A*, volume 89(5):053816 (2014).
- [Kofman12] KOFMAN, A.G.; ASHHAB, S. AND NORI, F. ‘Nonperturbative theory of weak pre- and post-selected measurements.’ In: *Physics Reports*, volume 520(2):43 – 133 (2012). Nonperturbative theory of weak pre- and post-selected measurements.
- [Leggett89] LEGGETT, A. ‘Comment on “how the result of a measurement of a component of the spin of a spin-(1/2) particle can turn out to be 100”.’ In: *Physical review letters*, volume 62(19):2325 (1989).
- [Lundeen09] LUNDEEN, J. AND STEINBERG, A. ‘Experimental joint weak measurement on a photon pair as a probe of hardy’s paradox.’ In: *Physical review letters*, volume 102(2):020404 (2009).
- [Lundeen11] LUNDEEN, J.S.; SUTHERLAND, B.; PATEL, A.; STEWART, C. AND BAMBER, C. ‘Direct measurement of the quantum wavefunction.’ In: *Nature*, volume 474(7350):188 (2011).
- [Lundeen12] LUNDEEN, J.S. AND BAMBER, C. ‘Procedure for direct measurement of general quantum states using weak measurement.’ In: *Physical review letters*, volume 108(7):070402 (2012).
- [Malik14] MALIK, M.; MIRHOSSEINI, M.; LAVERY, M.P.; LEACH, J.; PADGETT, M.J. AND BOYD, R.W. ‘Direct measurement of a 27-dimensional orbital-angular-momentum state vector.’ In: *Nature communications*, volume 5:3115 (2014).

- [Martínez-Rincón17] MARTÍNEZ-RINCÓN, J.; MULLARKEY, C.A.; VIZA, G.I.; LIU, W.T. AND HOWELL, J.C. ‘Ultrasensitive inverse weak-value tilt meter.’ In: *Optics letters*, volume 42(13):2479–2482 (2017).
- [Massar11] MASSAR, S. AND POPESCU, S. ‘Estimating preselected and postselected ensembles.’ In: *Physical Review A*, volume 84(5):052106 (2011).
- [Meschede09] MESCHÉDE, D. *Optik, Licht und Laser*. Springer-Verlag (2009).
- [Michelson31] MICHELSON, A.A. AND LAUE, M.V. ‘Die relativbewegung der erde gegen den lichtäther.’ In: *Naturwissenschaften*, volume 19(38):779–784 (1931).
- [Oreshkov15] ORESHKOV, O. AND CERF, N.J. ‘Operational formulation of time reversal in quantum theory.’ In: *Nature Physics*, volume 11(10):853 (2015).
- [Peres89] PERES, A. ‘Quantum measurements with postselection.’ In: *Physical review letters*, volume 62(19):2326 (1989).
- [Qiu17] QIU, X.; XIE, L.; LIU, X.; LUO, L.; LI, Z.; ZHANG, Z. AND DU, J. ‘Precision phase estimation based on weak-value amplification.’ In: *Applied Physics Letters*, volume 110(7):071105 (2017).
- [Ravon07] RAVON, T. AND VAIDMAN, L. ‘The three-box paradox revisited.’ In: *Journal of Physics A: Mathematical and Theoretical*, volume 40(11):2873 (2007).
- [Resch04] RESCH, K.J.; LUNDEEN, J.S. AND STEINBERG, A.M. ‘Experimental realization of the quantum box problem.’ In: *Physics Letters A*, volume 324(2-3):125–131 (2004).
- [Saleh91] SALEH, B.E.; TEICH, M.C. AND SALEH, B.E. *Fundamentals of photonics*, volume 22. Wiley New York (1991).
- [Schlosshauer05] SCHLOSSHAUER, M. ‘Decoherence, the measurement problem, and interpretations of quantum mechanics.’ In: *Reviews of Modern physics*, volume 76(4):1267 (2005).

- [Schlosshauer13] SCHLOSSHAUER, M.; KOFLER, J. AND ZEILINGER, A. ‘A snapshot of foundational attitudes toward quantum mechanics.’ In: *Studies in History and Philosophy of Science Part B: Studies in History and Philosophy of Modern Physics*, volume 44(3):222–230 (2013).
- [Simon11] SIMON, C. AND POLZIK, E.S. ‘Fock-state view of weak-value measurements and implementation with photons and atomic ensembles.’ In: *Physical Review A*, volume 83(4):040101 (2011).
- [Singh18] SINGH, A.; RAY, S.; CHANDEL, S.; PAL, S.; MANDAL, A.; MITRA, P. AND GHOSH, N. ‘Observation of weak value amplification in polarization-tailored fano interference in waveguided plasmonic crystals.’ In: *Bulletin of the American Physical Society* (2018).
- [Sokolovski13] SOKOLOVSKI, D. ‘Are the ‘weak measurements’ really measurements?’ In: *arXiv preprint arXiv:1305.4809* (2013).
- [Sokolovski16] SOKOLOVSKI, D. ‘Weak measurements measure probability amplitudes (and very little else).’ In: *Physics Letters A*, volume 380(18-19):1593–1599 (2016).
- [Svensson13] SVENSSON, B.E. ‘What is a quantum-mechanical “weak value” the value of?’ In: *Foundations of Physics*, volume 43(10):1193–1205 (2013).
- [Svensson14] SVENSSON, B.E. ‘On the interpretation of quantum mechanical weak values.’ In: *Physica Scripta*, volume 2014(T163):014025 (2014).
- [Tanaka13] TANAKA, S. AND YAMAMOTO, N. ‘Information amplification via postselection: A parameter-estimation perspective.’ In: *Physical Review A*, volume 88(4):042116 (2013).
- [Vaidman17] VAIDMAN, L.; BEN-ISRAEL, A.; DZIEWIOR, J.; KNIPS, L.; WEISSL, M.; MEINECKE, J.; SCHWEMMER, C.; BER, R. AND WEINFURTER, H. ‘Weak value beyond conditional expectation value of the pointer readings.’ In: *Physical Review A*, volume 96(3):032114 (2017).
- [Vaughan89] VAUGHAN, M. *The Fabry-Perot interferometer: history, theory, practice and applications*. CRC press (1989).

- [Wiseman09] WISEMAN, H.M. AND MILBURN, G.J. *Quantum measurement and control*. Cambridge university press (2009).
- [Yokota09] YOKOTA, K.; YAMAMOTO, T.; KOASHI, M. AND IMOTO, N. ‘Direct observation of hardy’s paradox by joint weak measurement with an entangled photon pair.’ In: *New Journal of Physics*, volume 11(3):033011 (2009).
- [Zilberberg11] ZILBERBERG, O.; ROMITO, A. AND GEFEN, Y. ‘Charge sensing amplification via weak values measurement.’ In: *Physical review letters*, volume 106(8):080405 (2011).

Declaration of Authorship:

I, Katharina Senkalla, hereby declare that this thesis is my own work, and that I have not used any sources and aids other than those stated in the thesis.

Hiermit erkläre ich, Katharina Senkalla, die vorliegende Arbeit selbständig verfasst zu haben und keine anderen als die in der Arbeit angegebenen Quellen und Hilfsmittel benutzt zu haben.

Munich, _____

Signature: _____